Faculty of Physics
WARSAW UNIVERSITY OF TECHNOLOGY

# Advances in Relativistic Heavy-Ion Physics

*a personal selection of recent experimental results*

Łukasz Graczykowski

5th Symposium of the Division for Physics of Fundamental Interactions of the Polish Physical Society
Katowice, Poland
21 October 2022

# Disclaimer

- This talk is based on two excellent (and longer) overviews by:
  - Catalin Ristea (link)
  - Gian Michele Innocenti (link)
  - ...+ additional material

- Great overview of the current status of the field can be found by looking at the material from two major conferences:
  - Quark Matter (QM 2022) in Kraków (link)
  - Strangeness in Quark Matter (SQM 2022) in Busan (link)

- QCD predicts at high temperature/density the quark-gluon plasma (QGP): a deconfined system of quarks and gluons
- QGP might have existed in the expanding Universe in the first μs after the Big Bang
  - Achieved in the laboratory by colliding heavy ions

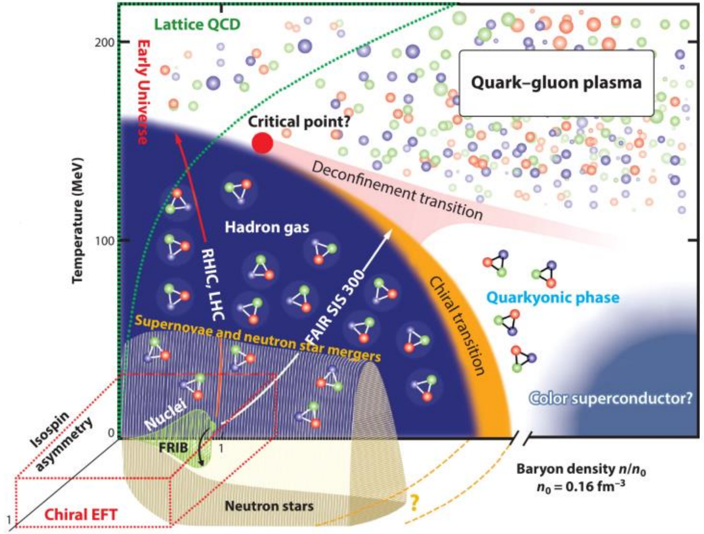

- QCD predicts at high temperature/density the quark-gluon plasma (QGP): a deconfined system of quarks and gluons
- QGP might have existed in the expanding Universe in the first μs after the Big Bang
    - **Achieved in the laboratory by colliding heavy ions**

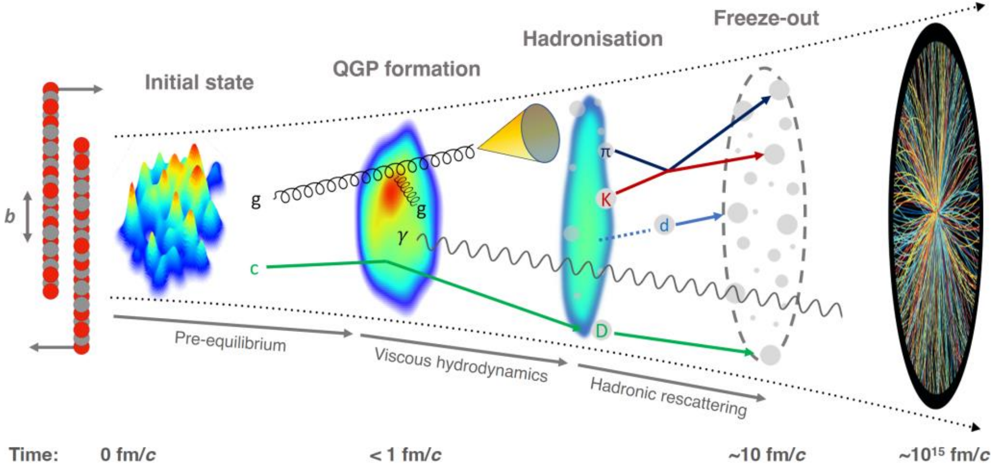


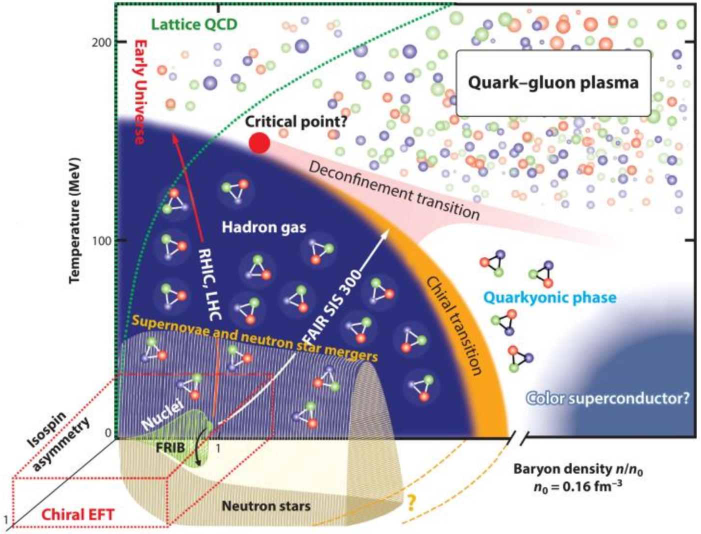


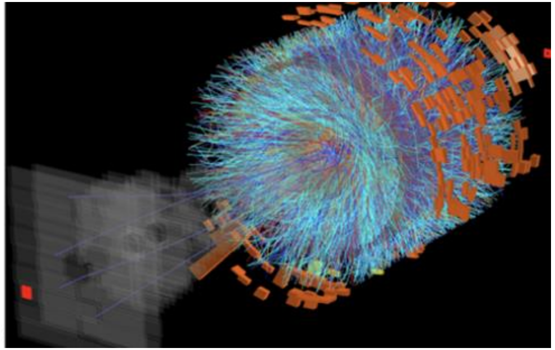

| RUN I 2009-2013 | LS1 | RUN 2 2015-2018 | LS2 | RUN 3 2022-2025 | LS3 | RUN 4 2029-2032 |
|---|---|---|---|---|---|---|
| pp, p-Pb, Pb-Pb | | pp, p-Pb, Xe-Xe, Pb-Pb | | pp, p-O, O-O, p-Pb, Pb-Pb | | pp, p-Pb, Pb-Pb |

**A-A**

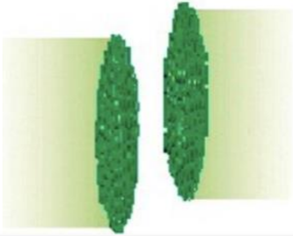

"*hot/dense QCD matter*"
**final state effects**
thermal and collective particle production (flow)

**p-A**

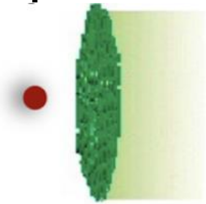

"*cold nuclear matter*"
**initial state effects**
shadowing and gluon saturation

**pp**

"*vacuum*"
**reference**

Exciting physics also in
**high multiplicity pp and p-A collisions**

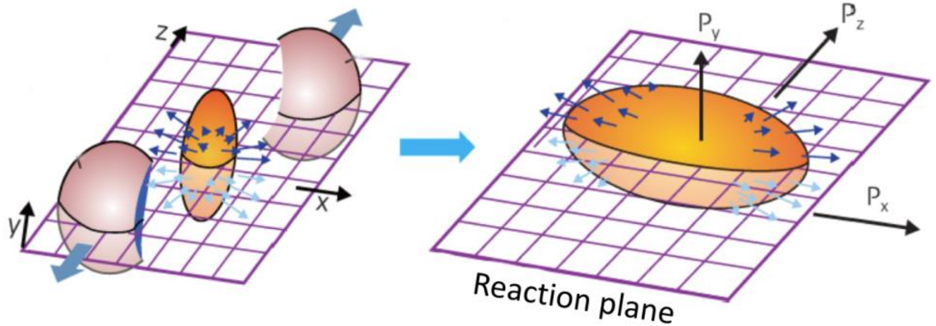


Anisotropic flow: the transfer of initial spatial anisotropy into the final anisotropy in momentum space via collective interactions

$$E\frac{d^3N}{d^3p}=\frac{1}{2\pi}\frac{d^2N}{p_T\,dp_T\,dy}\left(1+\sum_{n=1}^{\infty}2v_n\cos\left[n(\phi-\Psi_n)\right]\right)$$

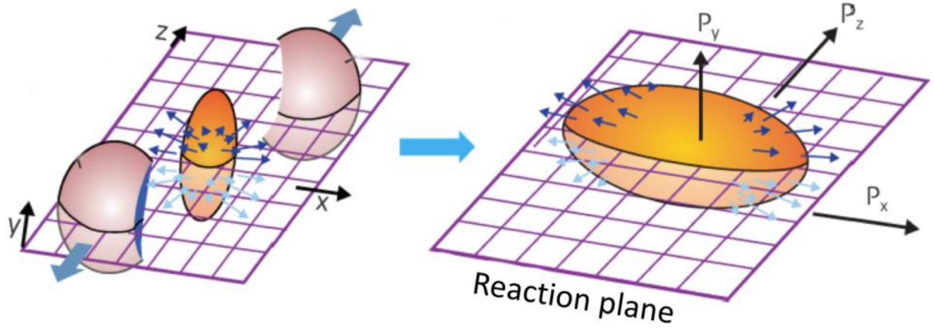


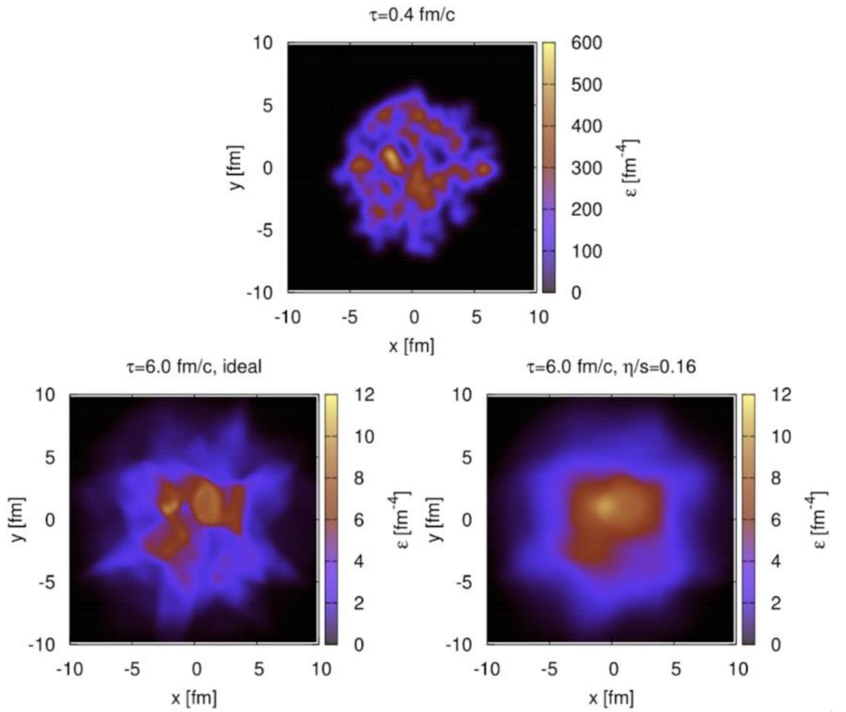


Anisotropic flow: the transfer of initial spatial anisotropy into the final anisotropy in momentum space via collective interactions

$$E\frac{d^3N}{d^3p}=\frac{1}{2\pi}\frac{d^2N}{p_T\,dp_T\,dy}\left(1+\sum_{n=1}^{\infty}2v_n\cos[n(\phi-\Psi_n)]\right)$$

Sensitive to the system evolution

- Constrain initial conditions, equation-of-state,transport properties
- Stronger constraints are obtained from measurements of identified particles

$R_{AA}$ = 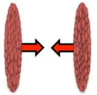 / ($N_{coll}$ × )

$$R_{AA} = \frac{1}{N_{coll}} \frac{dN/dp_T(AA)}{dN/dp_T(pp)}$$

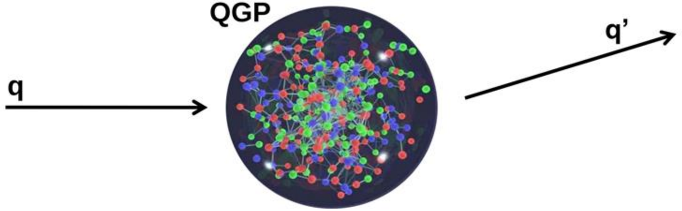


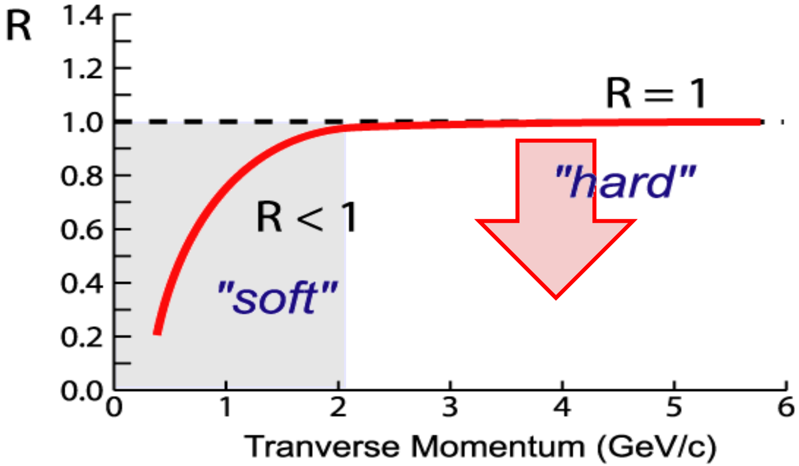


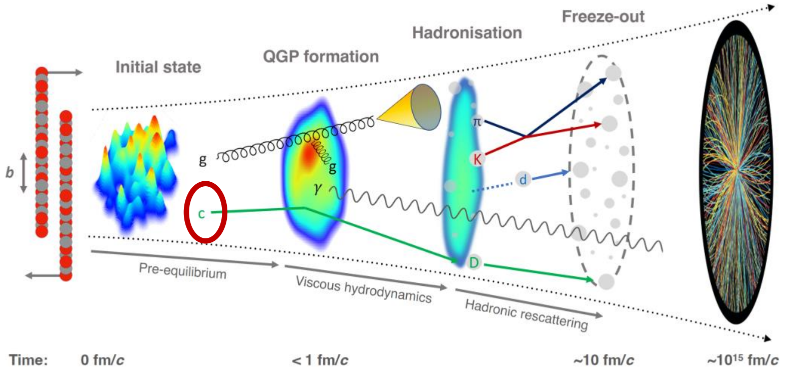


$R_{AA} < 1$ at high $p_T$ – nuclear effects suppress the particle production
$R_{AA} \sim 1$ at high $p_T$ (binary scaling) – no nuclear effects

Heavy quarks are produced early in the evolution, before QGP is formed, therefore are an excellend probe

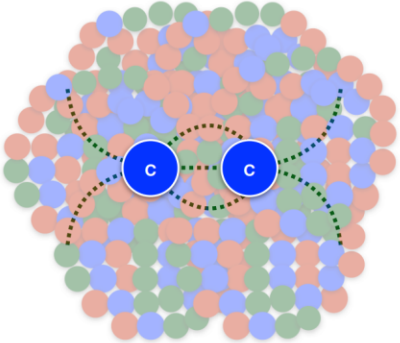

$R_{AA} = \frac{\text{[A–A collision]}}{N_{coll} \times \text{[p–p collision]}}$

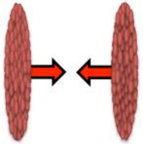

Color screening → dissociation

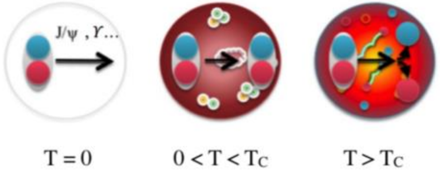


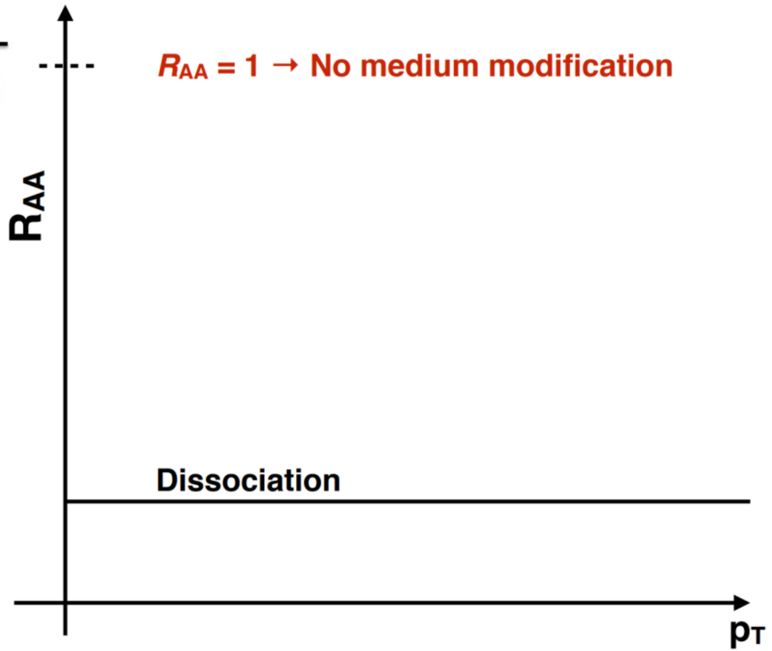


- **Dissociation:**
  - J/ψ melt inside the medium **(colour screening)**

Phys.Lett.B 178 (1986) 416-422

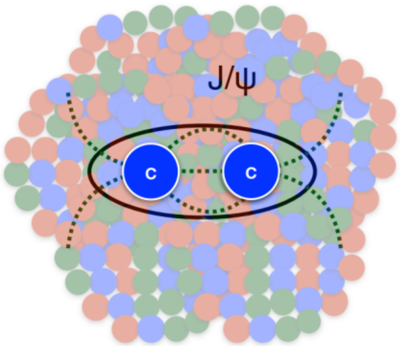


$$R_{AA} = \frac{\text{[A–A collision]}}{N_{coll} \times \text{[p–p collision]}}$$

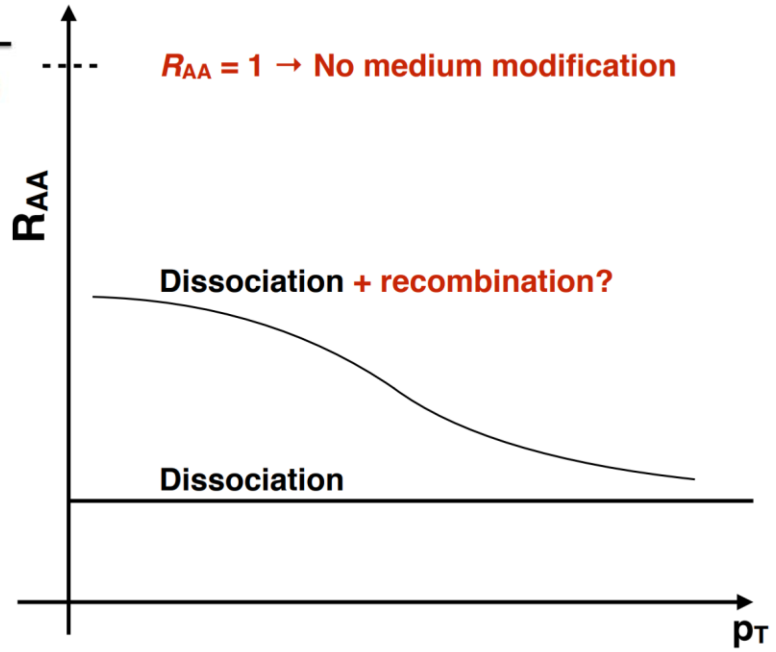


- **Dissociation:**
  - J/ψ melt inside the medium **(colour screening)**
- **Recombination:**
  - J/ψ created in the QGP by combination of c-cbar pairs

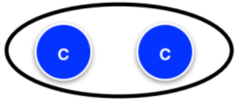

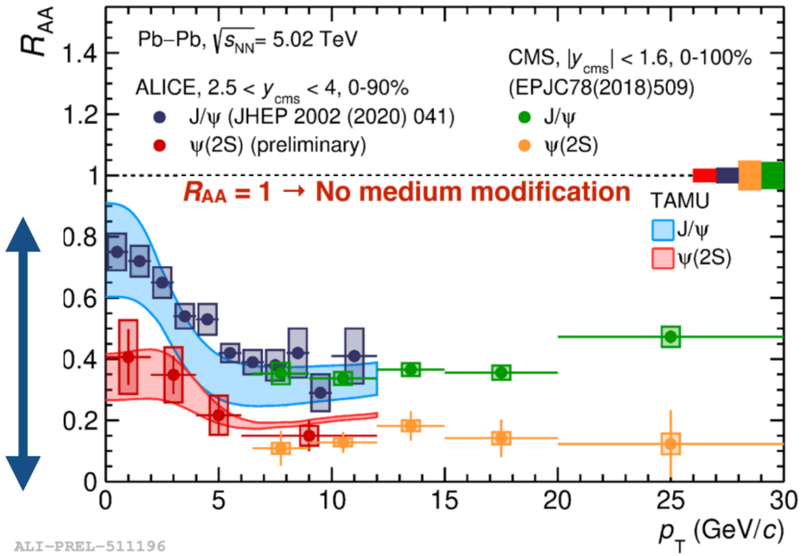


**Inclusive J/Ψ, Ψ(2S)**

- Stronger suppression at high-$p_T$ and increasing trend of $R_{AA}$ towards low-$p_T$ for both charmonium states → hint of regeneration
- Good agreement between CMS and ALICE in the common $p_T$ range

**Effects of recombination:**

- overall **enhancement of the $R_{AA}$ at low $p_T$**
- more J/ψ at **central rapidities** than at **forward rapidities:**

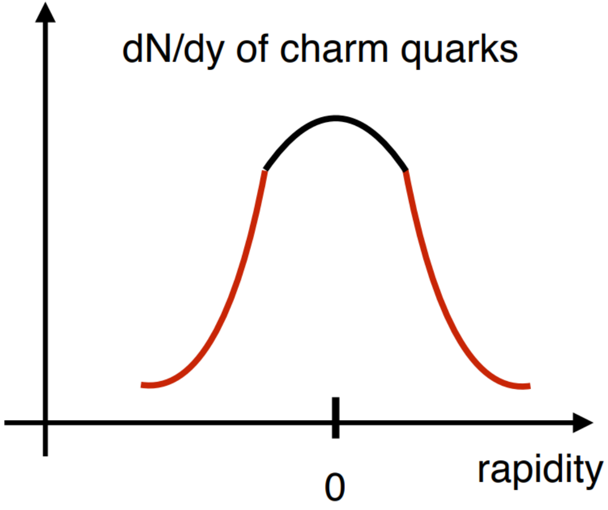

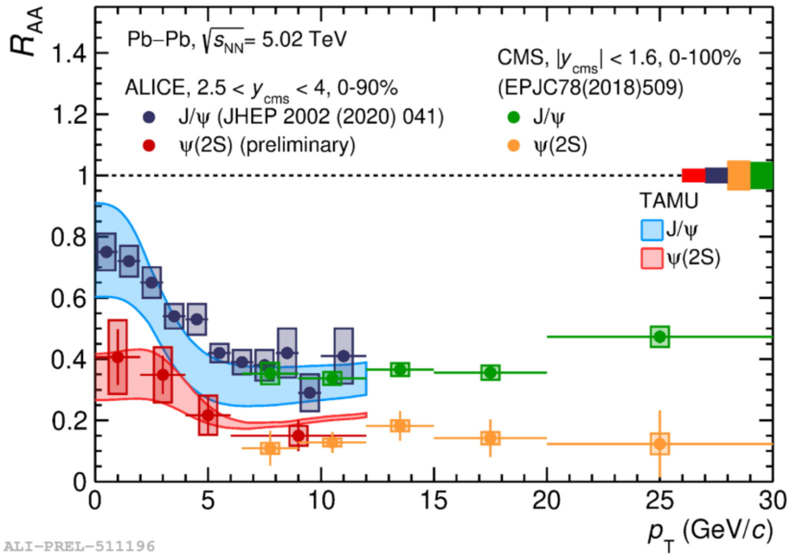


CMS-PAS-HIN-21-008

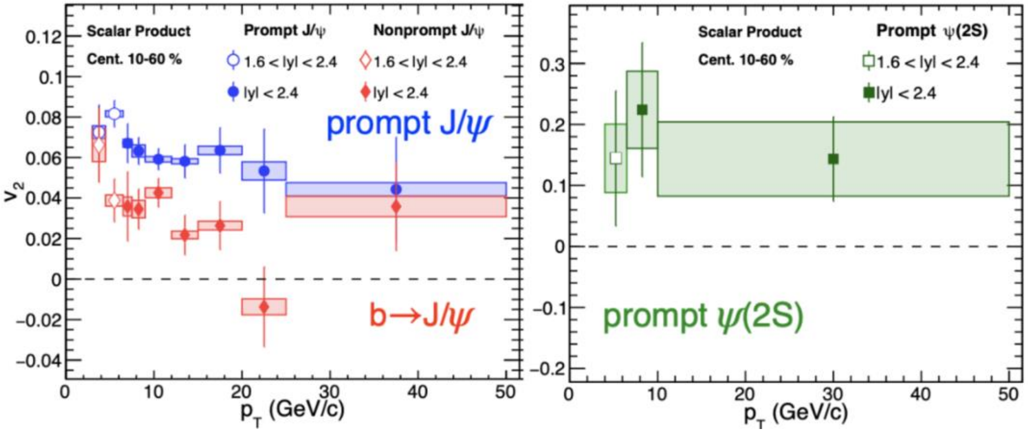


**Inclusive J/Ψ, Ψ(2S)**

- Stronger suppression at high-$p_T$ and increasing trend of $R_{AA}$ towards low-$p_T$ for both charmonium states → hint of regeneration
- Good agreement between CMS and ALICE in the common $p_T$ range

**Prompt J/Ψ**

- Significant $v_2$ up to high-$p_T$
- b→J/Ψ has lower $v_2$ and decreases faster

**Ψ(2S) $v_2 \gtrsim 0.1$ > J/Ψ $v_2$**

- Hint of different regeneration contribution for ground and excited states

Phys. Rev. C 95 (2017) 034908

Bottomonia less affected by recombination due to lower b-bbar cross section!

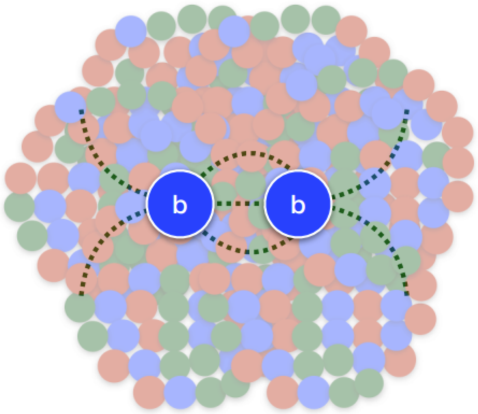


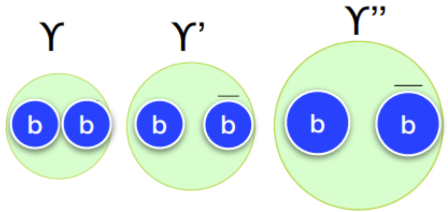


different radii/binding energies
→ **different suppression**

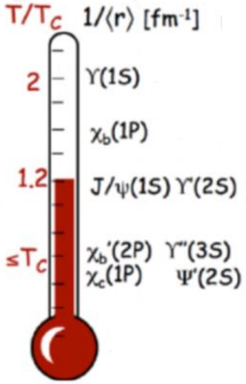


QGP "Thermometer"

A. Mocsy, EPJ C61, 705 (2009)

- **Dissociation:**
  - Bottomonia melt inside the medium **(colour screening)**

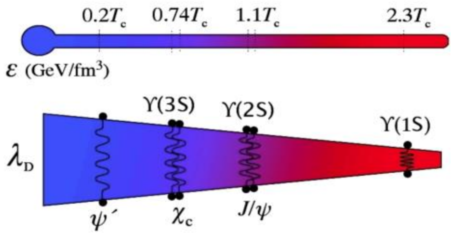

Bottomonia less affected by recombination due to lower b-bar cross section!

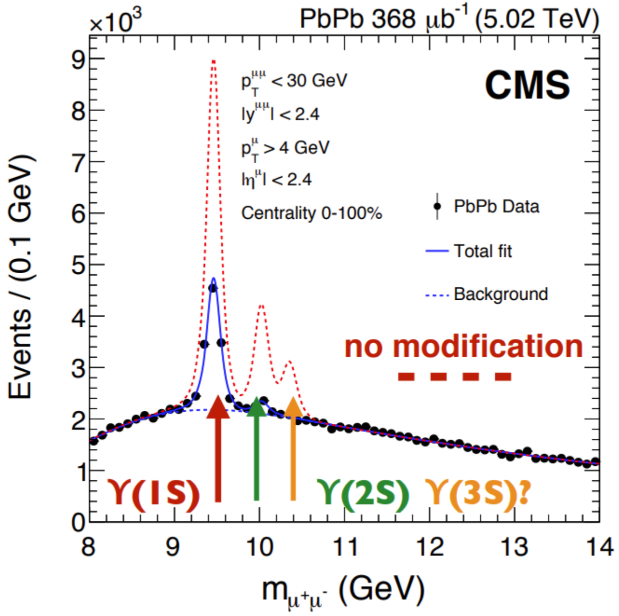


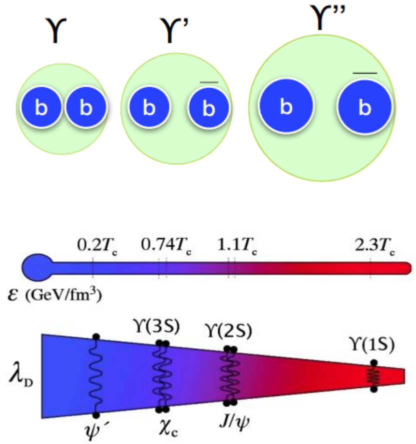


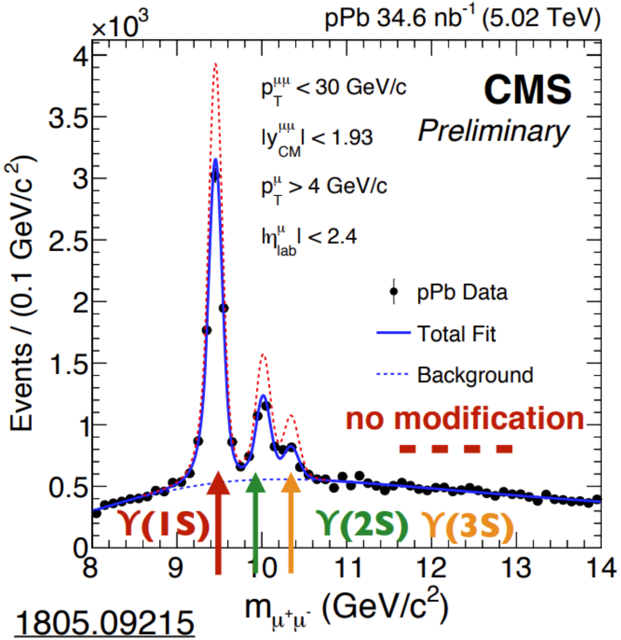


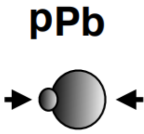


1805.09215

- Strong suppression w.r.t. to pp collisions in PbPb collisions!
- Loosely bound states more suppressed

- (Milder) Υ suppression of loosely bound states
- Need for **final state effects in pPb collisions (e.g. hadronic rescattering)**

**How much of the PbPb suppression can be explained by "cold" final state processes?**

JHEP10 (2018) 094

# Υ(3S), first time observation in PbPb

*PLB 790 (2019) 270*

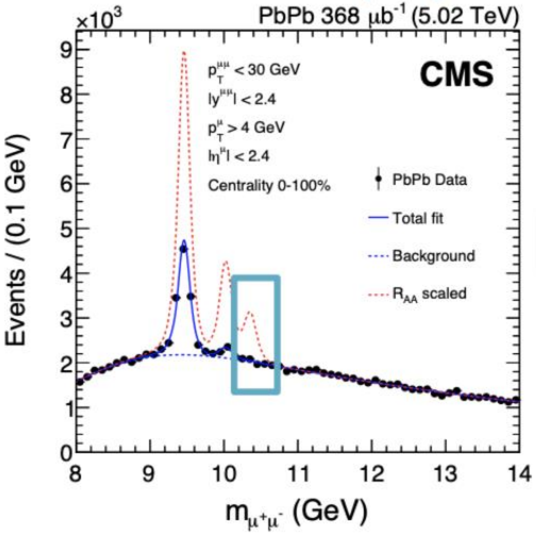


CMS-PAS-HIN-21-007

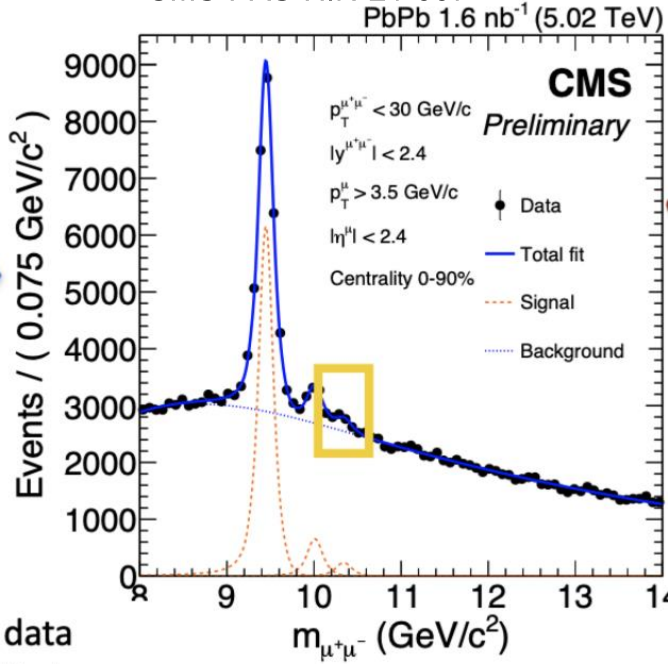


2015 data: **370 $\mu$b-1**,
No clear Υ(3S) peak

x4.3 more data
& BDT applied

2018 data: 1600 $\mu$b-1,
Significance above $5\sigma$

High statistic data is really important

CMS-PAS-HIN-21-007

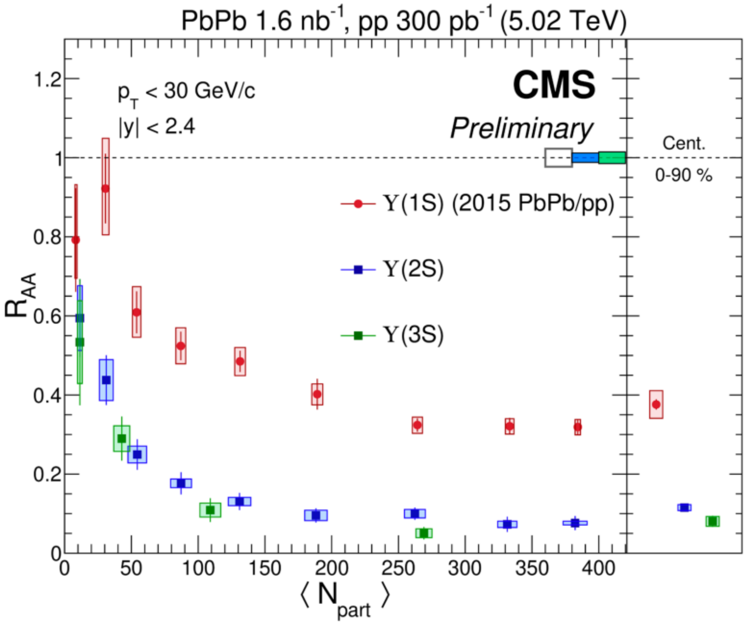


**Υ(1S) $R_{AA}$ >> Υ(2S) $R_{AA}$ ≳ Υ(3S) $R_{AA}$**

Sequential melting of Υ(ns) states

See also ATLAS: arXiv:2205.03042

# Υ(nS) measurements

CMS-PAS-HIN-21-007

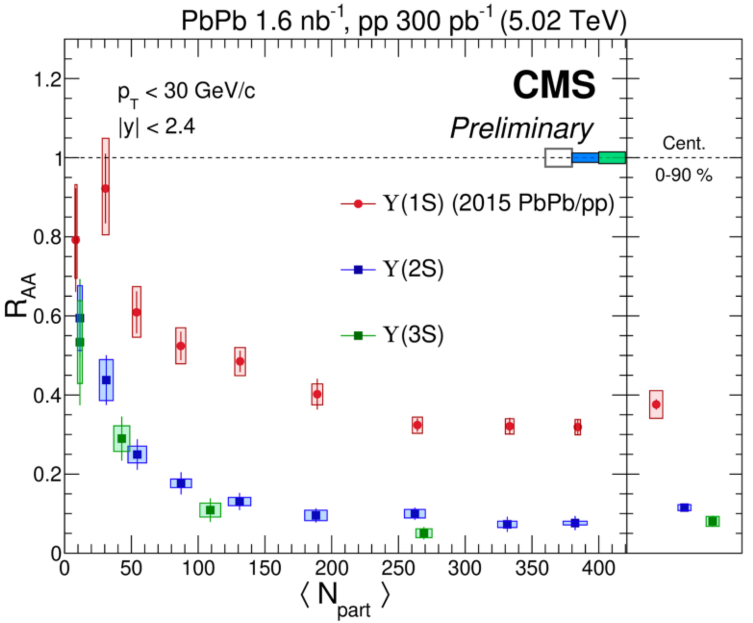


CMS, PLB 819 (2021) 136385

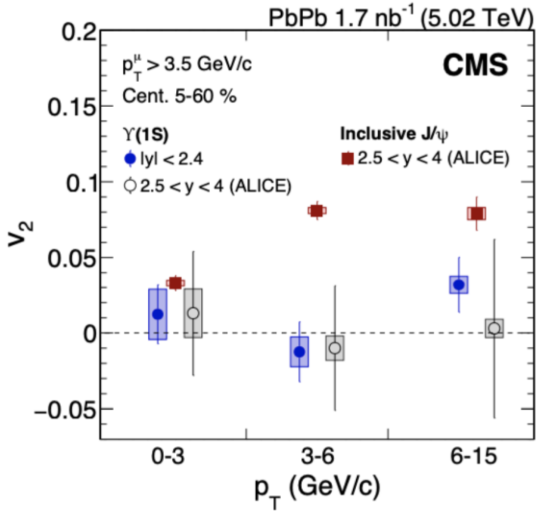


CMS-PAS-HIN-21-001

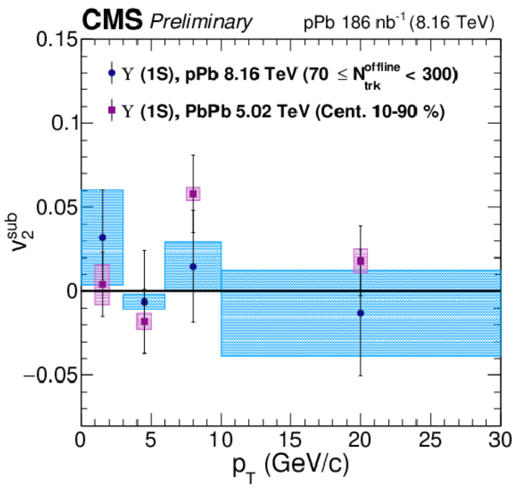


**Υ(1S) $R_{AA}$ >> Υ(2S) $R_{AA}$ ≳ Υ(3S) $R_{AA}$**

Sequential melting of Υ(ns) states

See also ATLAS: arXiv:2205.03042

**0 ~ Υ(1S) $v_2^{\text{HM p-Pb}}$ ~ Υ(1S) $v_2^{\text{Pb-Pb}}$ < J/Ψ $v_2$**

Υ's strong binding make itself less sensitive to initial geometry

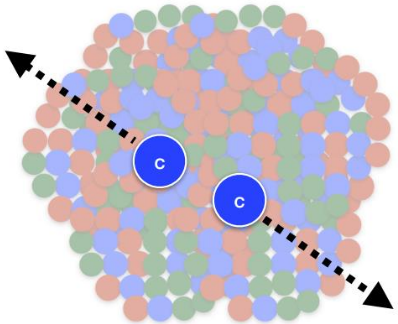
c
c

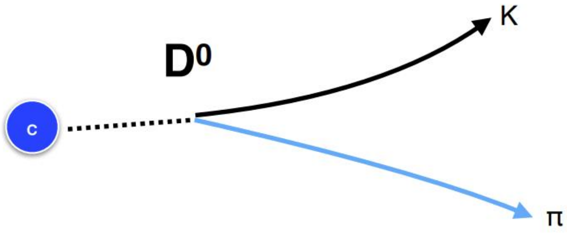
c
D0
K
π

In-medium energy loss as a consequence of **radiative** and **collisional** processes.

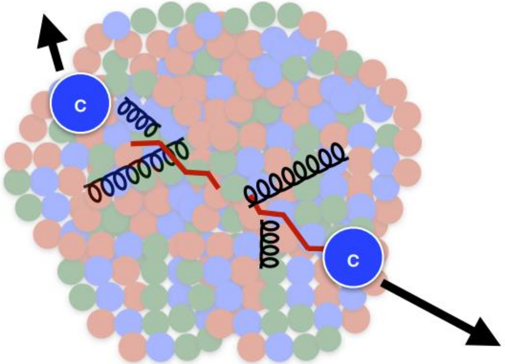


**QCD predicts modifications in the presence of QGP due to:**

- different Casimir factors for quarks vs gluons
- dead cone effect:

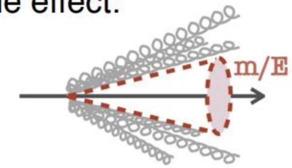


**ALICE direct observation of dead cone**
Nature 605, 440-446 (2022)

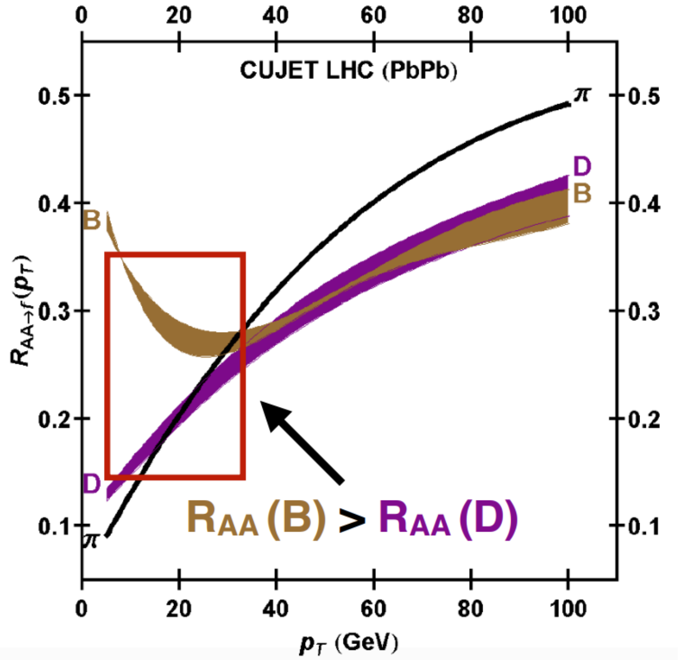


→ $E_{loss}$ (gluon) > $E_{loss}$ (charm) > $E_{loss}$ (beauty)

# Open charm - prompt $D^0$ meson

ALICE, JHEP 01 (2022) 174

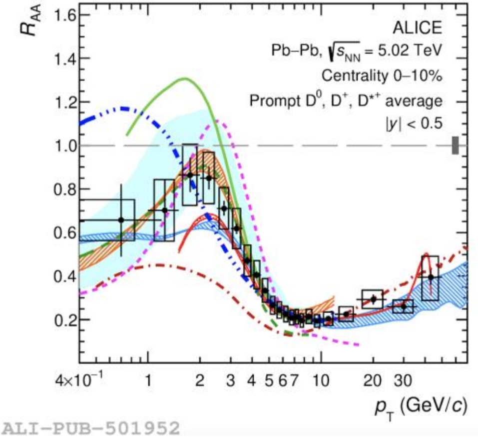


- Precise D meson measurements down to low $p_T$

ALICE, JHEP 01 (2022) 174

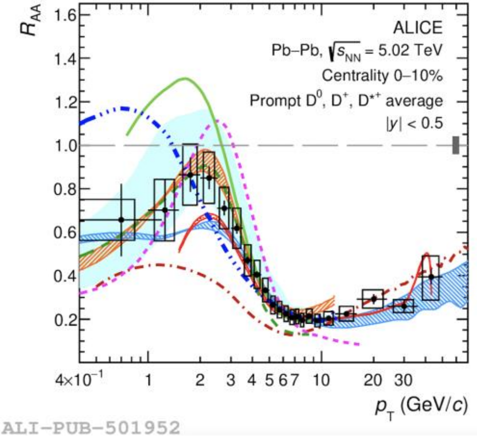


ALICE, arXiv:2112.08156

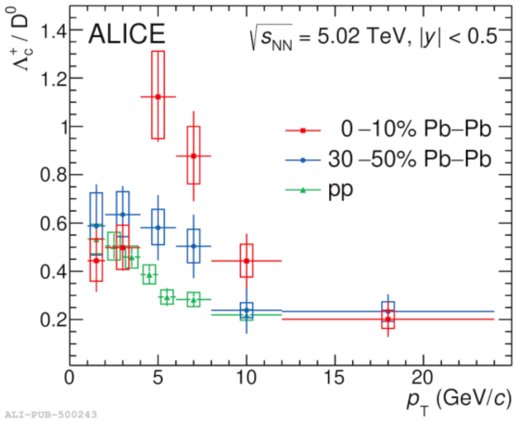


- Precise D meson measurements down to low $p_T$
- Additional constraints from $\Lambda_c$ measurements
  - Theory suggests enhancement of $\Lambda_c$/D ratio in Pb-Pb over pp
  - Enhancement due to hadronization by recombination + increase in the intermediate $p_T$ from collective expansion

# Open charm – prompt D⁰ meson

ALICE, JHEP 01 (2022) 174

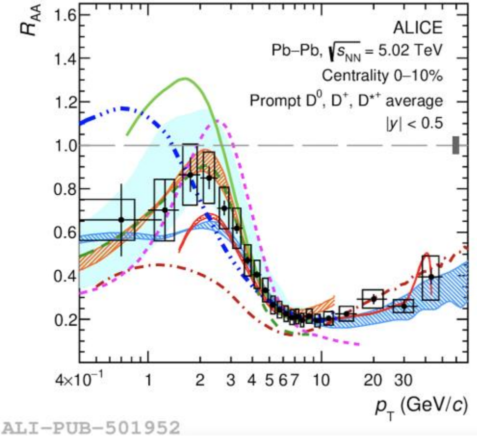


ALICE, arXiv:2112.08156

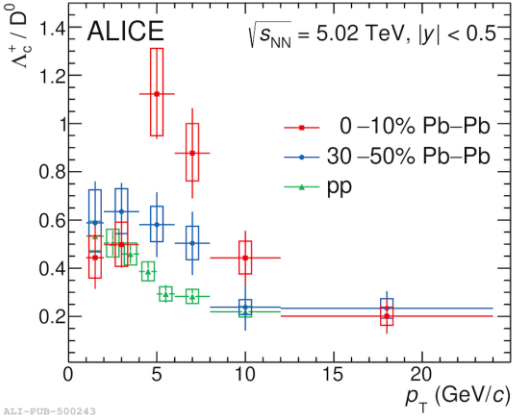


CMS, PRL 129 (2022) 022001
CMS, PLB 816 (2021) 136253

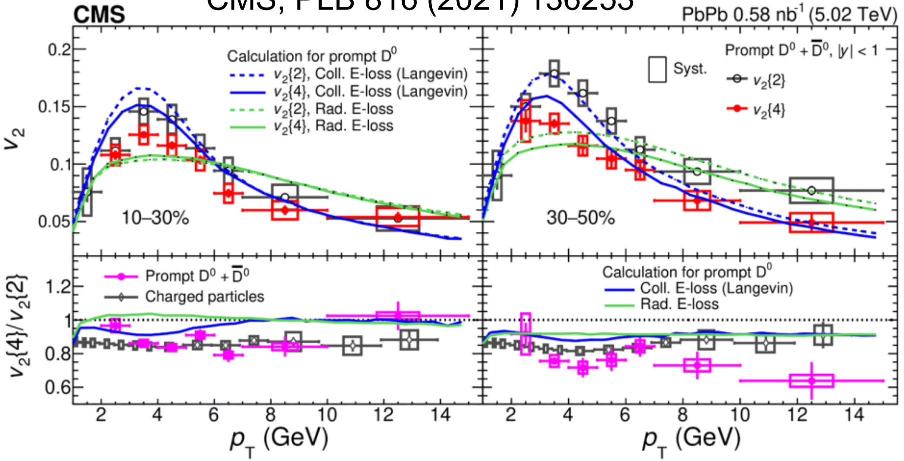


- Precise D meson measurements down to low $p_T$
- Additional constraints from $\Lambda_c$ measurements
  - Theory suggests enhancement of $\Lambda_c$/D ratio in Pb-Pb over pp
  - Enhancement due to hadronization by recombination + increase in the intermediate $p_T$ from collective expansion
- The elliptic flow of prompt D⁰ has similar pattern to that of charged hadrons
  → D mesons acquire additional flow via c and light quark recombination
- **Charm production suppressed in heavy-ion collisions and charm quark flows**

ALICE, arXiv:2202.00815

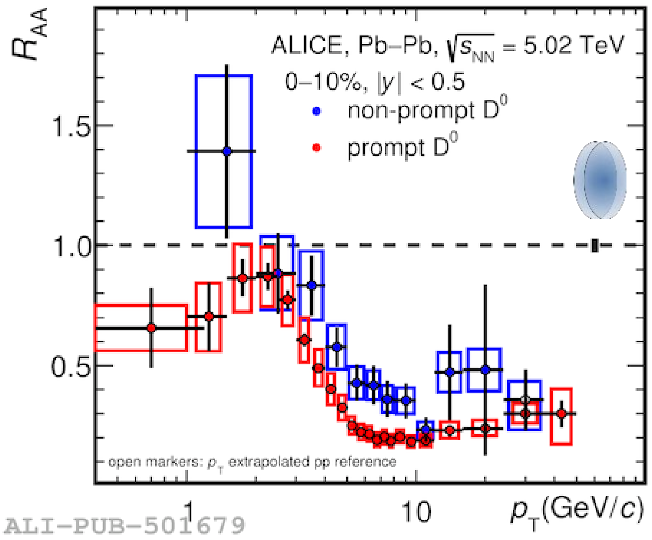


- Energy loss predicted to depend on QGP density, but also on quark mass
  - "Dead cone" effect reduces small-angle gluon radiation for high-mass quarks
- Less suppression for (non-prompt) $D^0$ mesons from B decays than prompt $D^0$ mesons

$$\mathbf{R_{AA}(b) > R_{AA}(c) \Rightarrow \mathit{E}_{loss}(b) < E_{loss}(c)}$$

# Prompt $D^0$ vs b $\rightarrow D^0$

ALICE, arXiv:2202.00815

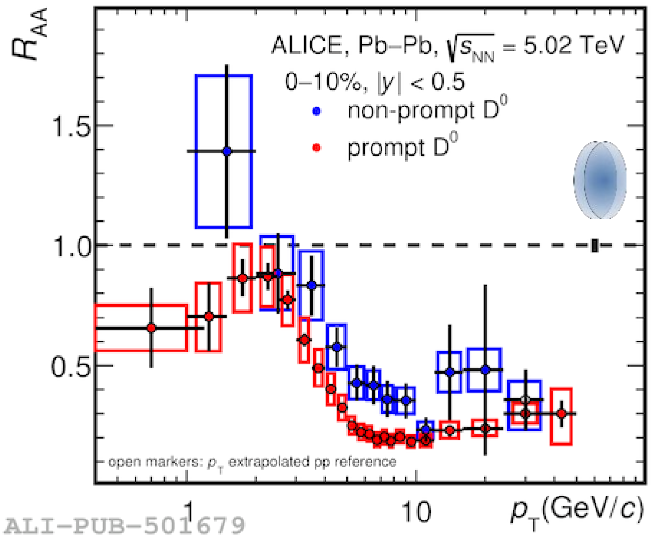


CMS-PAS-HIN-21-003

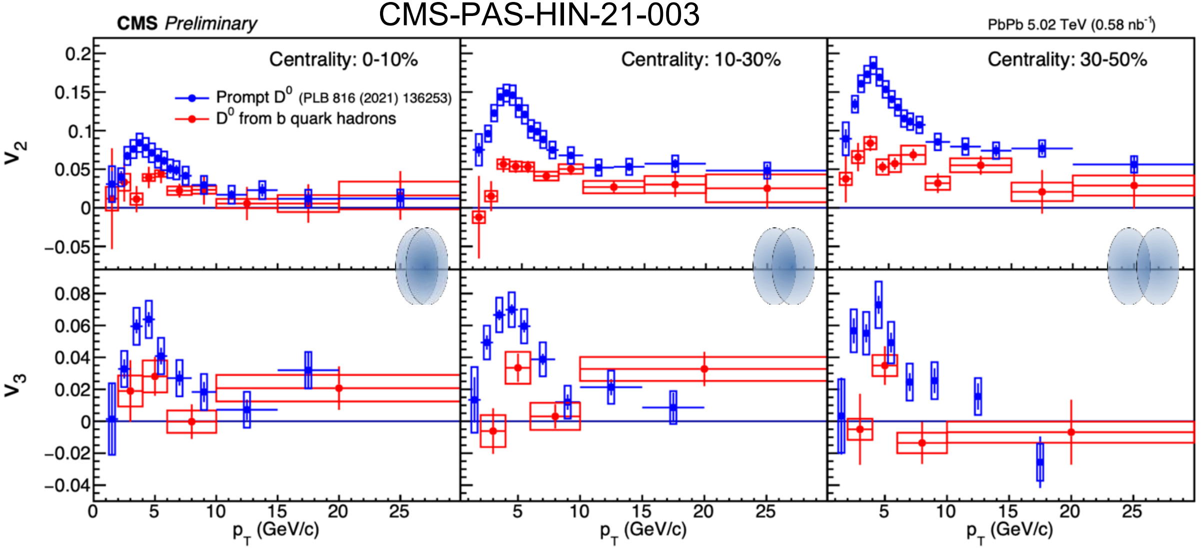


- Energy loss predicted to depend on QGP density, but also on quark mass
  - "Dead cone" effect reduces small-angle gluon radiation for high-mass quarks
- Less suppression for (non-prompt) $D^0$ mesons from B decays than prompt $D^0$ mesons

$$\mathbf{R_{AA}(b) > R_{AA}(c) \Rightarrow \mathit{E}_{loss}(b) < E_{loss}(c)}$$

- Non-zero $v_2$ observed → b-quarks partially thermalise in the medium or recombine with light quarks
- Significant non-zero $v_3$ for b → $D^0$ for all centrality bins → b hadron collectivity is sensitive to fluctuation of initial geometry

CMS-PAS-HIN-21-008

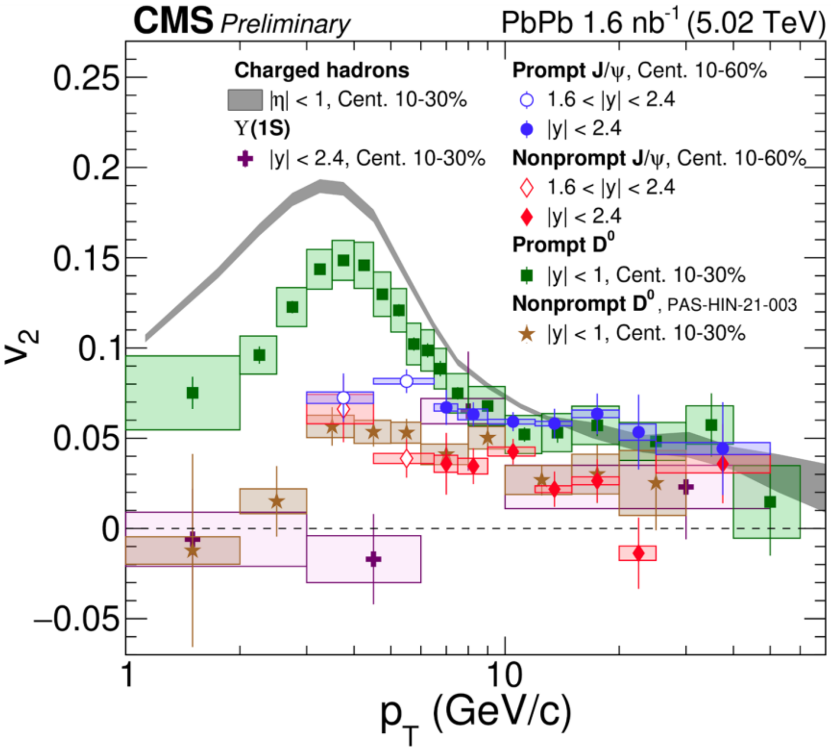


- Comprehensive picture of elliptic flow in Pb-Pb collisions
- Low $p_T$: step increase following mass hierarchy hydrodynamic regime

**light quarks > charm > beauty**

- Maximum $v_2$ reached at $3 < p_T < 6$ GeV/c:

**light quarks ≳ prompt D$^0$ > prompt J/Ψ > b→hadrons**
→ coalescence of heavy quarks with light quarks at play

- High $p_T$: convergence toward non-zero $v_2$

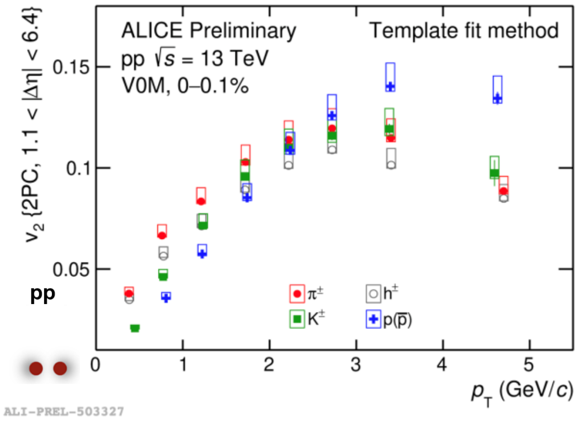


without quark coalescence

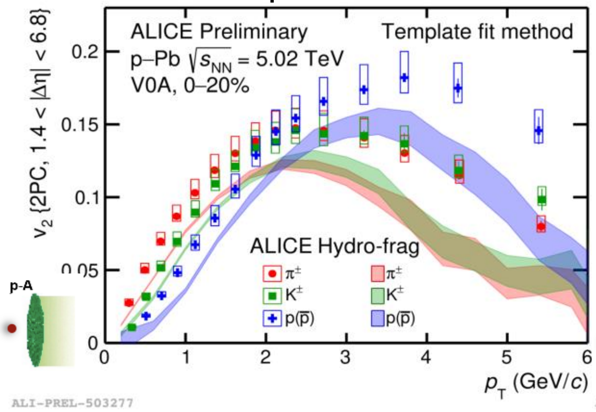


with quark coalescence

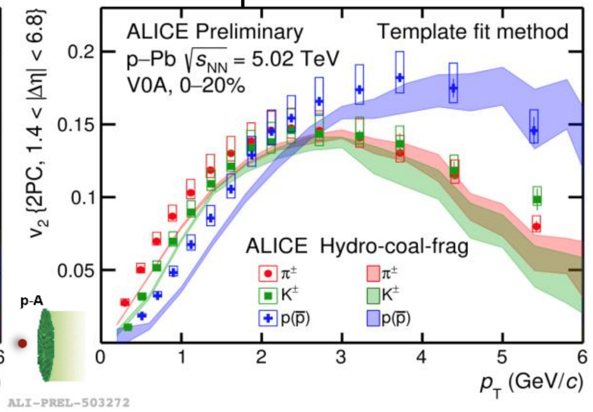


**Light flavors**: p-Pb model comparison indicates partonic flow + coalescence

→ baryon - meson grouping in both pp and p-Pb

→ quark-level flow + recombination in high-multiplicity p-Pb (and pp)

ALICE, arXiv: 2206.04587

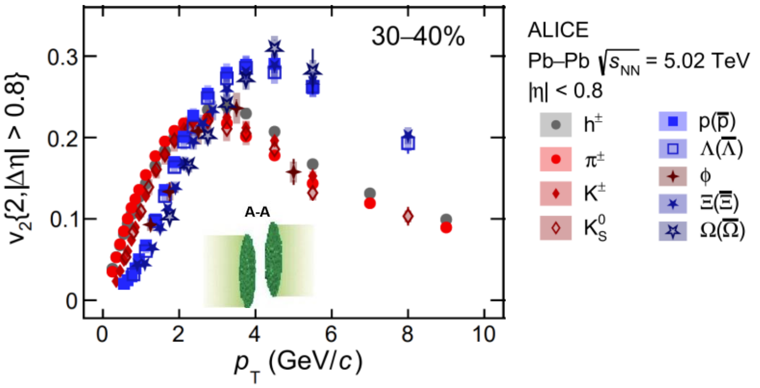

# Elliptic flow in small systems

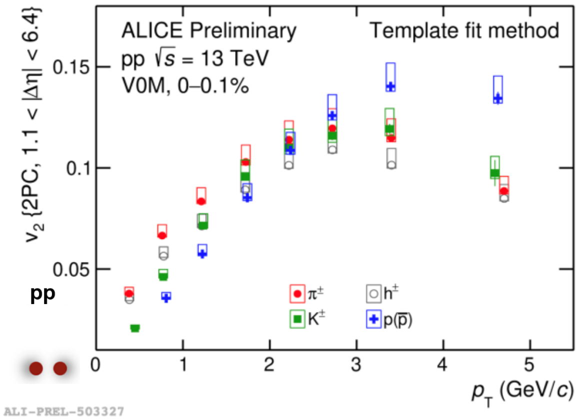


without quark coalescence

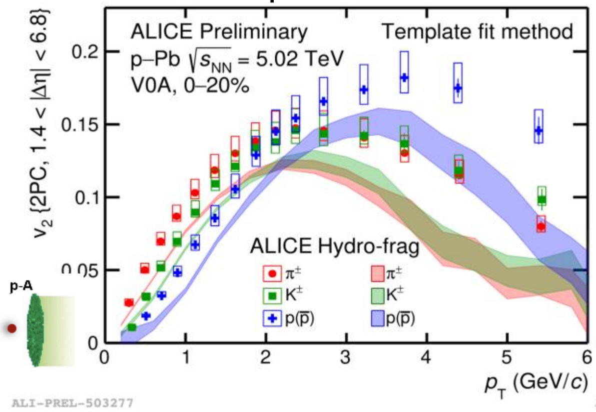


with quark coalescence

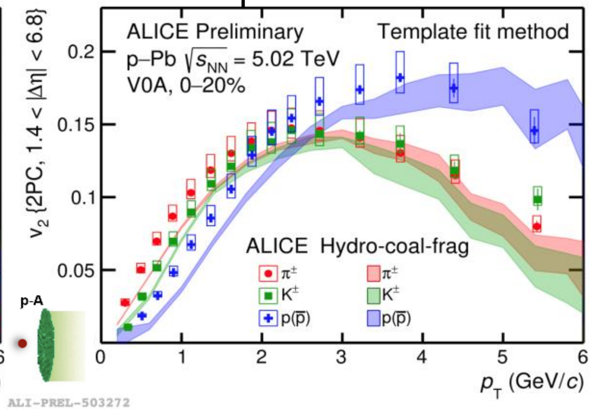


**Light flavors**: p-Pb model comparison indicates partonic flow + coalescence

→ baryon - meson grouping in both pp and p-Pb

→ quark-level flow + recombination in high-multiplicity p-Pb (and pp)

**Heavy flavors**: No significant $p_T$ dependence and $v_2^{J/\psi}$ in pp compatible with 0 ($v_2^{pp} < v_2^{p\text{-}Pb} < v_2^{Pb\text{-}Pb}$)

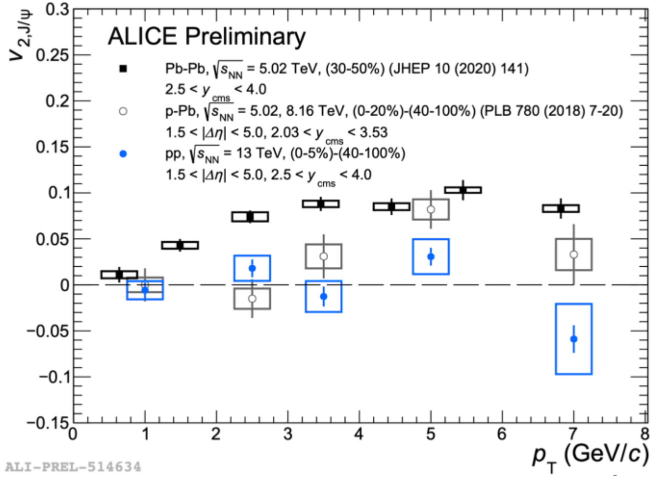

# Elliptic flow in small systems

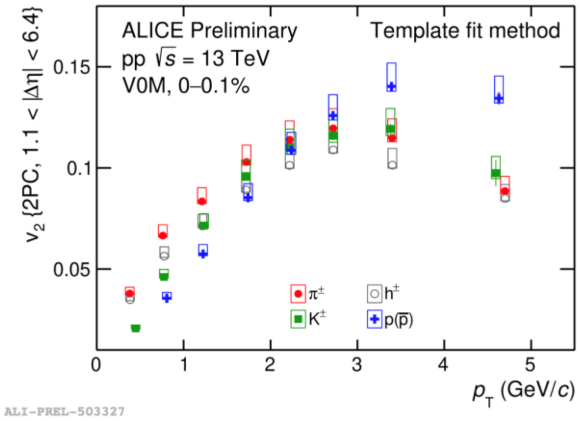


without quark coalescence

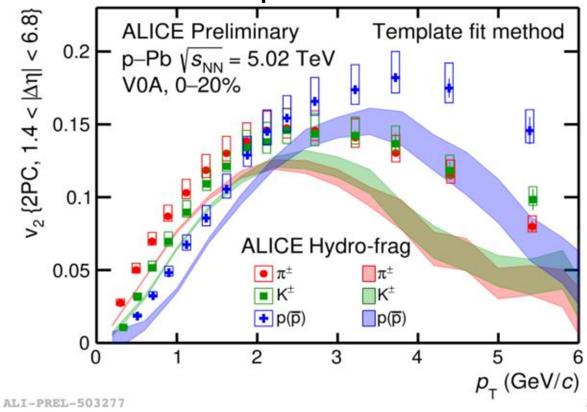


with quark coalescence

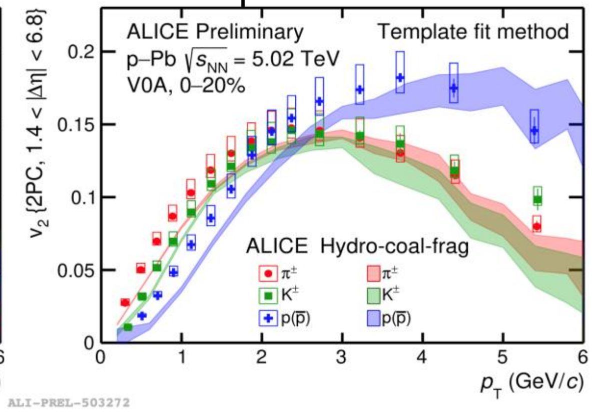


**Light flavors**: p-Pb model comparison indicates partonic flow + coalescence

→ baryon - meson grouping in both pp and p-Pb

→ quark-level flow + recombination in high-multiplicity p-Pb (and pp)

**Heavy flavors**: No significant $p_T$ dependence and $v_2^{J/\psi}$ in pp compatible with 0 ($v_2^{pp} < v_2^{p\text{-}Pb} < v_2^{Pb\text{-}Pb}$)

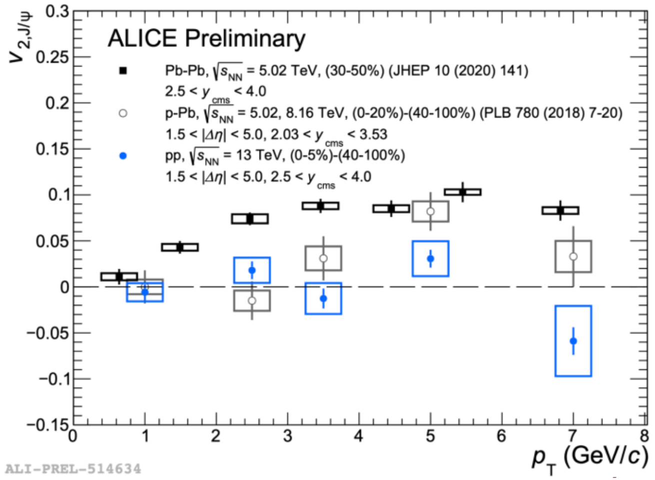


More small systems measurements:

ATLAS, PRC 104 (2021) 014903; CMS, arXiv:2204.13486

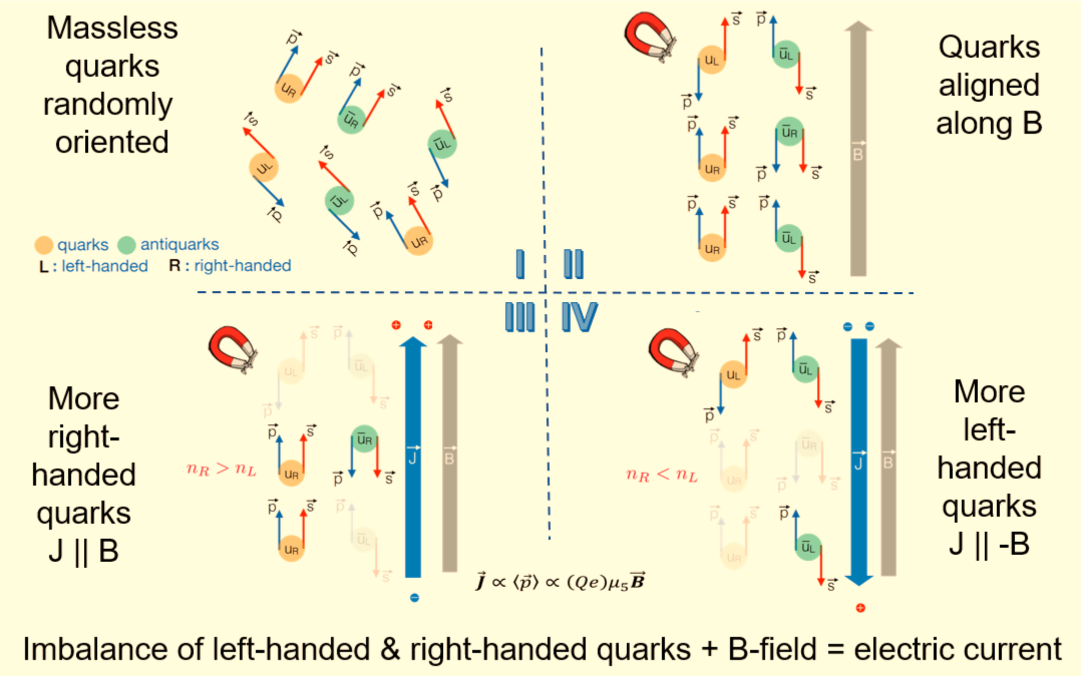


Chiral Magnetic Effect (CME) – imbalance of the right- and left-handed quarks – it arises from topological fluctuations in QCD, which are related to the local violation of P and CP

The magnetic fields in HI are on the order of $10^{17}$-$10^{18}$ Gauss and are the strongest magnetic fields observed in nature

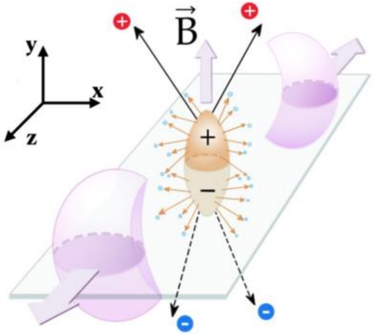


A charge current is induced along the magnetic field

$$\mathbf{j} = \frac{e^2}{2\pi^2}\mu_5 \mathbf{B}$$

This leads to charge separation wrt reaction plane

**Further reading:**

Kharzeev, McLerran, Warringa, Nucl.Phys.A 803 (2008) 227-253
Kharzeev et al, Phys.Lett.B 545 (2002) 298-306,
Mace et al, Phys. Rev. D 93, 074036 (2016),
Muller et. al., Phys. Rev. Lett. 117, 142301 (2016) ,
Lappi et al, Phys. Rev. D 97, 034034 (2018),
Skokov et al, Int.J.Mod.Phys.A 24 (2009) 5925-5932,
McLerran et al Nucl.Phys.A 929 (2014) 184-190

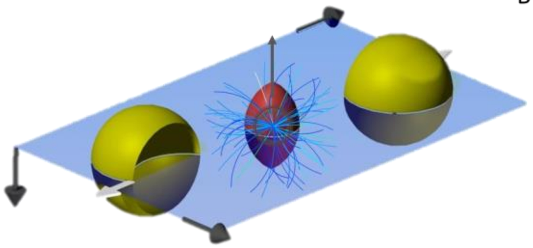

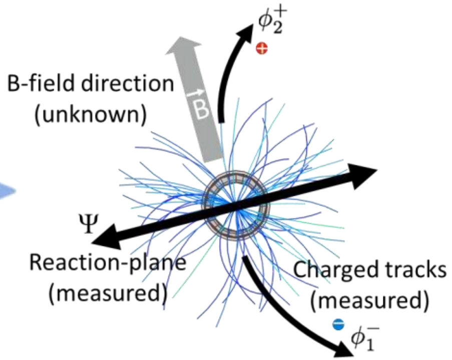


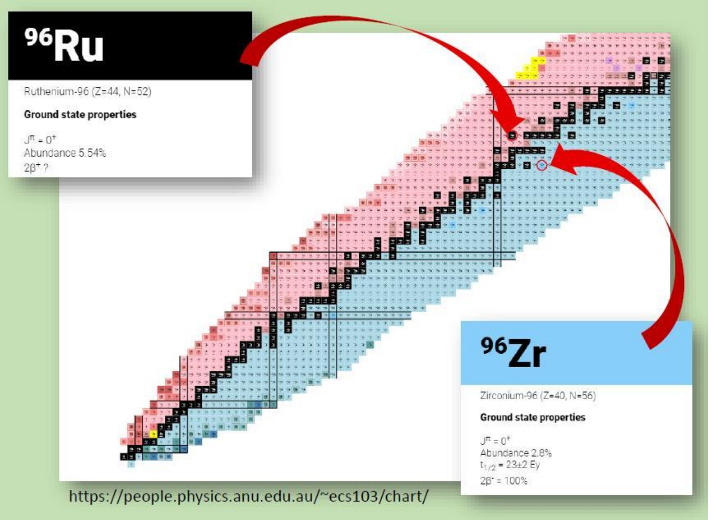


$$\gamma^{\alpha,\beta} \equiv \langle cos(\phi^{\alpha} + \phi^{\beta} - 2\psi_2)\rangle$$

$$\Delta\gamma = \gamma^{OS} - \gamma^{SS}$$

$$\Delta\gamma = \Delta\gamma^{CME} + k\frac{v_2}{N} + \Delta\gamma^{non-flow}$$

Measurement Signal Background 1 Background 2

$$\Delta\gamma^{Ru+Ru} = \Delta\gamma^{CME} + k\frac{v_2}{N} + \Delta\gamma^{non-flow}$$

$$\Delta\gamma^{Zr+Zr} = \Delta\gamma^{CME} + k\frac{v_2}{N} + \Delta\gamma^{non-flow}$$

$\boldsymbol{B}^2$ are ~15% different

Within 4%

CME effect should differ between those systems


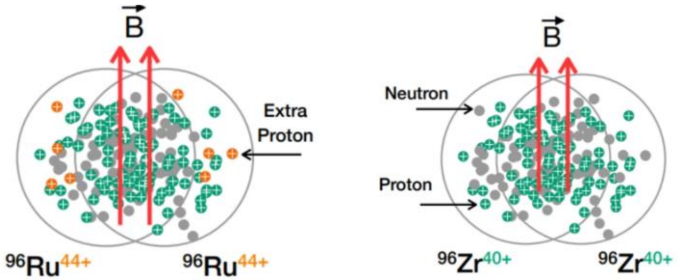



S. A. Voloshin, Phys. Rev. C70 (2004) 057901; S. A. Voloshin, Phys. Rev. Lett. 105 (2010) 172301; W.-T. Deng, et al Phys. Rev. C94 (2016) 041901; Khachatryan Vet al.(CMS) Phys. Rev. Lett.118 (2017) 122301; Adam J et al.(STAR) Phys. Lett. B 798 (2019) 134975

M. S. Abdallah *et al.* (STAR) Phys. Rev. C, 105 (2022) 014901

# 1. $\gamma$ measurement with full TPC ($|\eta| < 1$)

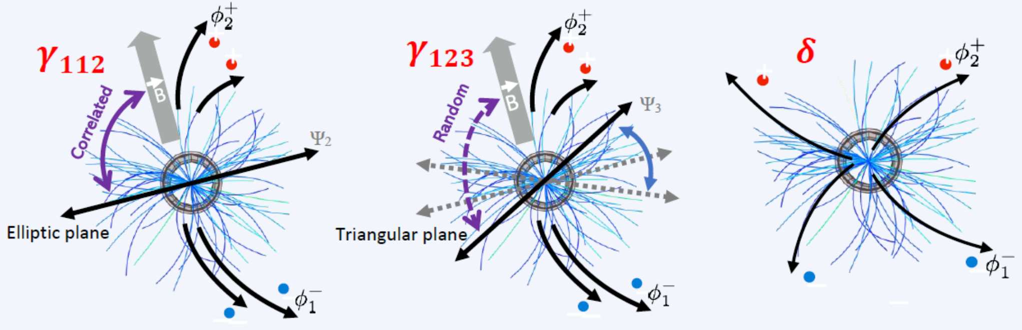


$$\gamma_{112} \equiv \left\langle \cos\left(\Phi_1(\eta_1) + \Phi_2(\eta_2) - 2\psi_2^{|\eta|<1}\right)\right\rangle$$

$$\gamma_{123} \equiv \left\langle \cos\left(\Phi_1(\eta_1) + 2\Phi_2(\eta_2) - 3\psi_3^{|\eta|<1}\right)\right\rangle$$

$$\delta = \langle \cos(\Phi_1 - \Phi_2)\rangle$$

**Pre-defined CME criteria:**

$$\frac{(\Delta\gamma_{112}/v_2)^{\mathrm{Ru+Ru}}}{(\Delta\gamma_{112}/v_2)^{\mathrm{Zr+Zr}}} > 1$$

$$\frac{(\Delta\gamma_{112}/v_2)^{\mathrm{Ru+Ru}}}{(\Delta\gamma_{112}/v_2)^{\mathrm{Zr+Zr}}} > \frac{(\Delta\gamma_{123}/v_3)^{\mathrm{Ru+Ru}}}{(\Delta\gamma_{123}/v_3)^{\mathrm{Zr+Zr}}}$$

$$\frac{(\Delta\gamma_{112}/v_2)^{\mathrm{Ru+Ru}}}{(\Delta\gamma_{112}/v_2)^{\mathrm{Zr+Zr}}} > \frac{(\Delta\delta)^{\mathrm{Ru+Ru}}}{(\Delta\delta)^{\mathrm{Zr+Zr}}}$$

Data not compatible with pre-defined CME criteria

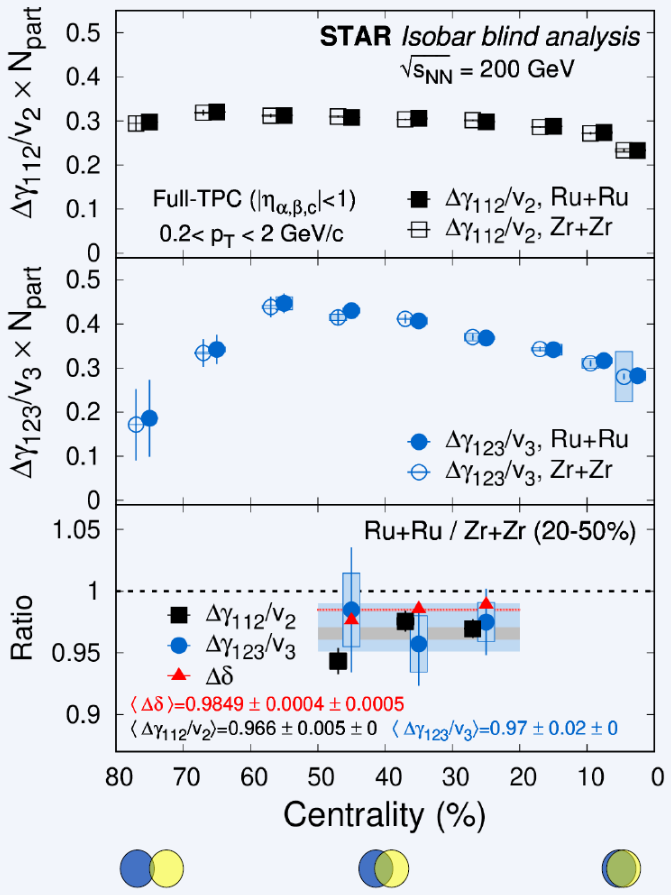

# CME results from RHIC/STAR

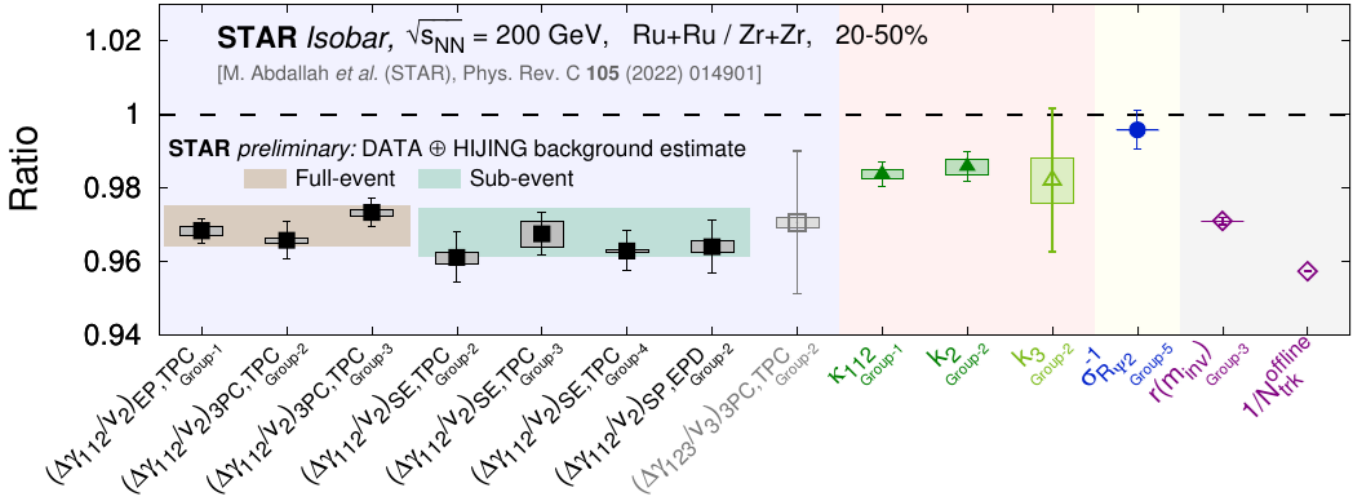


- CME criteria not met by the measurements

- No significant difference is observed for all the CME observables between two isobar systems
- $\Delta\gamma/v2$ratios are below unity - mainly driven by the multiplicity difference between the two isobars

- Further non-flow background studies shown at QM2022
- The isobar data are consistent with the current estimate of non-flow background within error

# Instead of a summary – the future

RUN I 2009-2013 | LS1 | RUN 2 2015-2018 | LS2 | RUN 3 2022-2025 | LS3 | RUN 4 2029-2032 | LS4 | RUN 5 2035-2038 | LS5 | RUN 6 2040-2041

**Next generation HI detector at the LHC**

**Compact all-silicon tracker**
→ clean separation of signal and background
**Vertex detector** with excellent pointing resolution
→ clean reconstruction of decay chains
**Particle identification**
→ background suppression
**Large acceptance**
→ statistics and correlations
**Superconducting magnet system**
→ effective provision of required magnetic field
**Continuous read-out and online processing**
→ large data sample to access rare signals

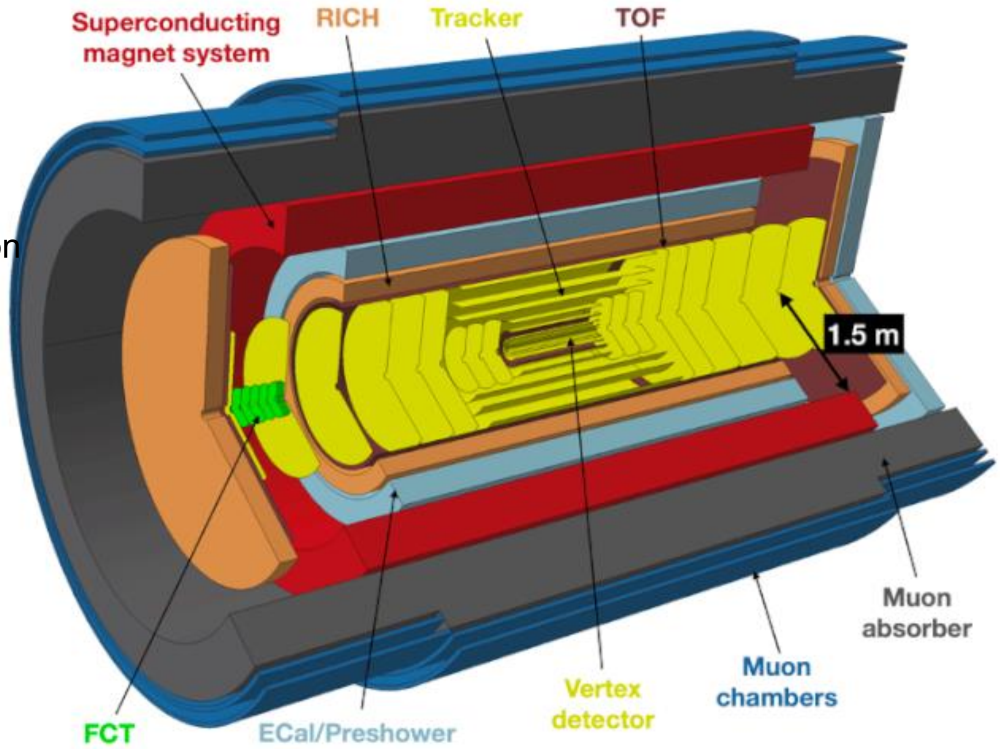

Standard Model and Beyond

21-23 October 2022
Katowice
Europe/Warsaw timezone

# THANK YOU

# BACKUP

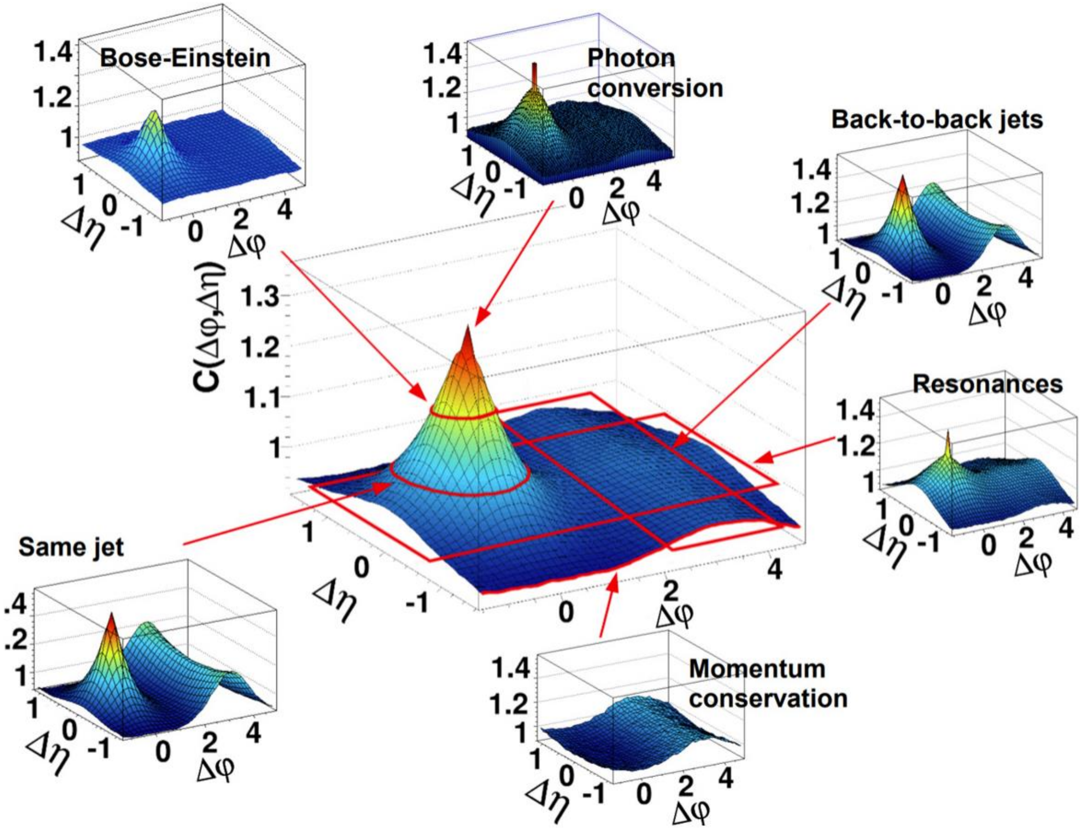


## Usually performed for charged hadrons

Used to extract flow coefficients or “ridge” studies

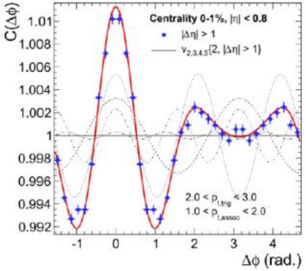


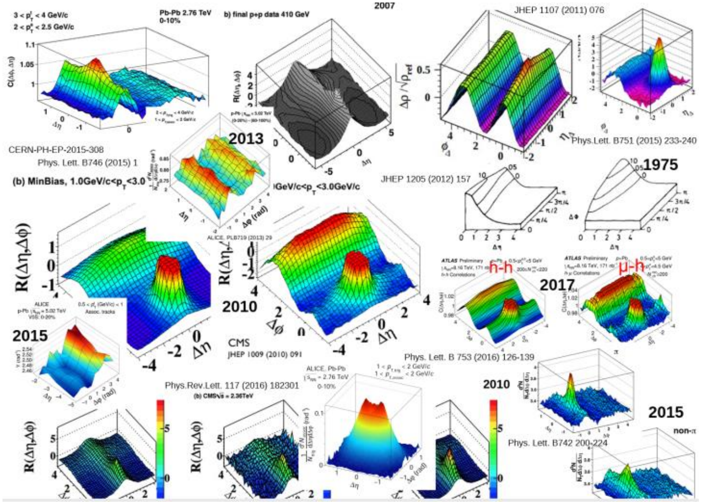

# Angular correlations of identified hadrons - puzzle

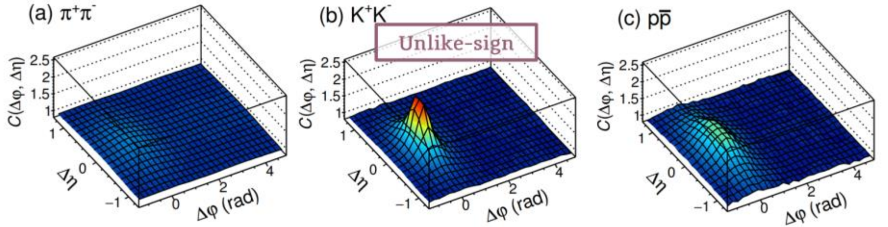


ALCE, Eur.Phys.J. C77 (2017) 8, 569

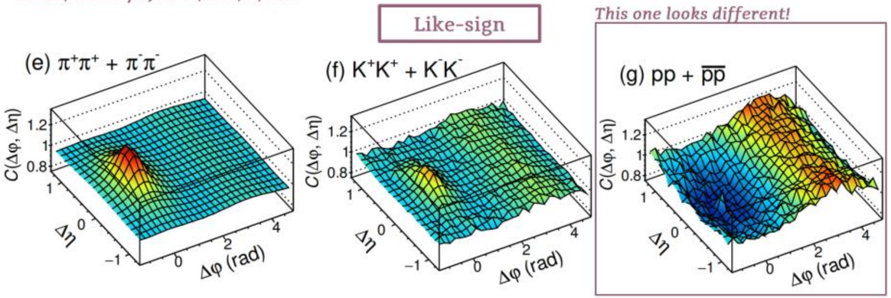


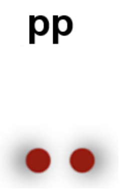


Possible reasons:
~~- (mini)jet collimation~~
~~- resonances~~
~~- quantum statistics~~
~~- FSI (strong, Coulomb)~~
~~- conservation laws (charge, strangeness, baryon number)~~
+momentum cons.

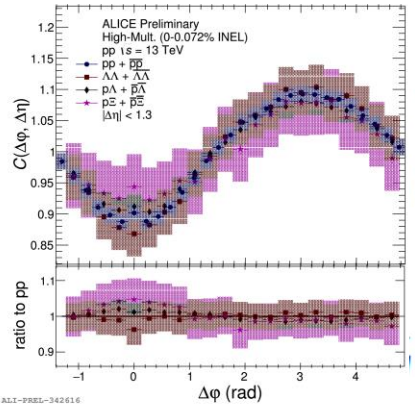


STAR, Phys. Rev. C 101, 014916 (2020)

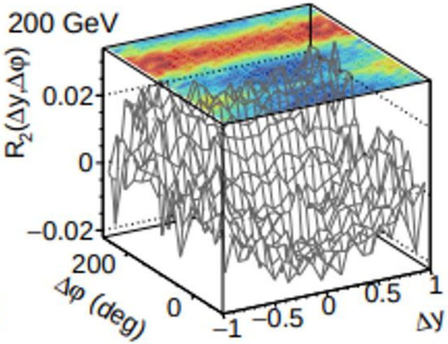


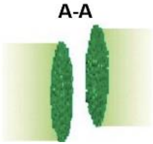


Ł. Graczykowski

Zhang et al., Phys. Rev. C 99, 054904 (2019)
AMPT model new developments

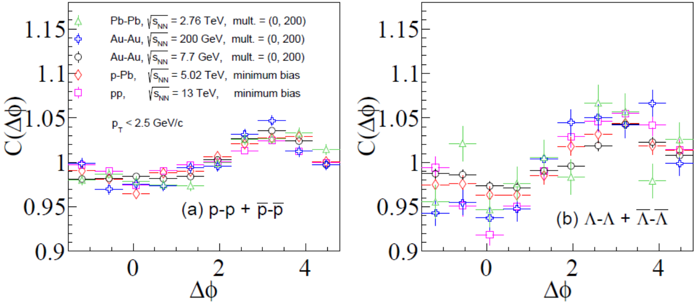

# Nuclear modification factor in p-Pb collisions

LHCb, Phys.Rev.Lett. 128 (2022), 142004

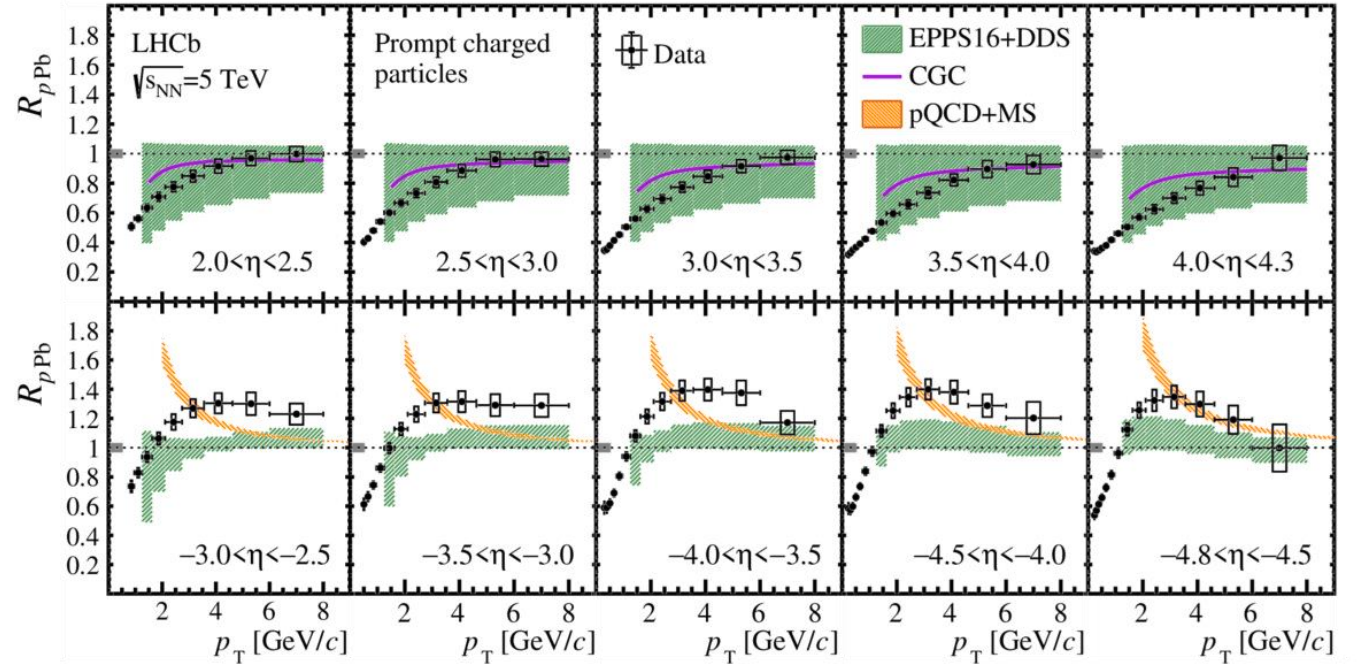


Complementary measurements in backward and forward η regions

**Forward region**
a suppression is observed, especially for low $p_T$
**Backward region**
significant enhancement for high $p_T$

Clear pseudorapidity dependence
→ Differences with CGC calculations at the lowest $p_T$
→ Multiple scattering calculations fail to describe the backward region

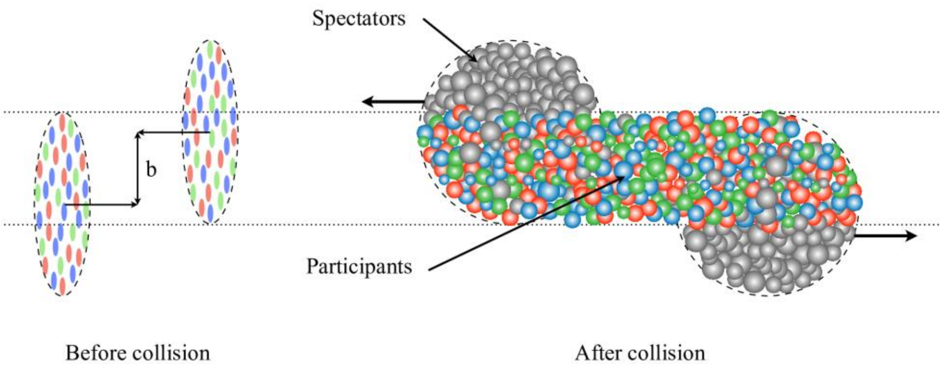


**Impact parameter b**

Perpendicular to beam direction
Connects centers of colliding nuclei
*Not measured directly* → estimated by centrality

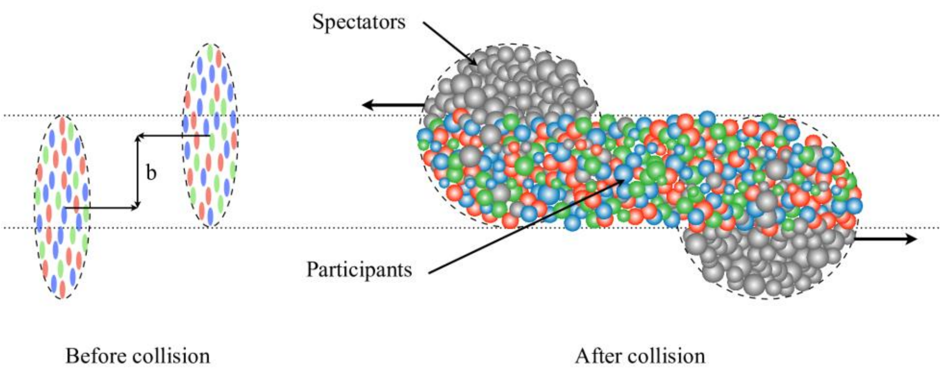


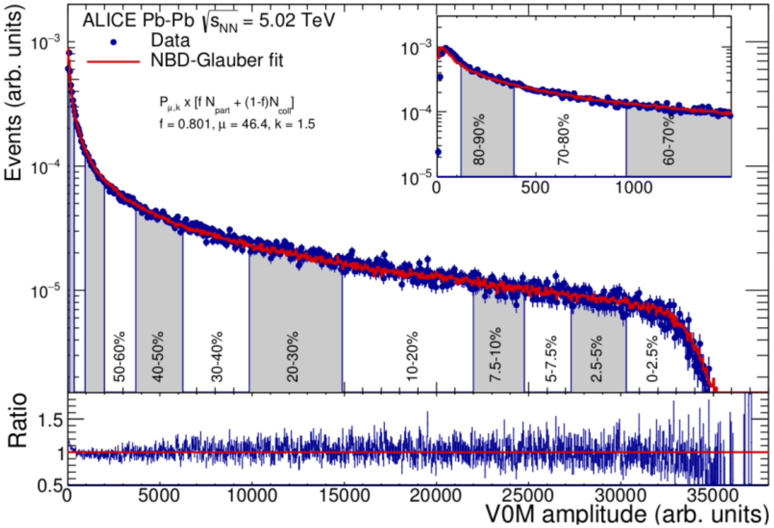


**Impact parameter b**

Perpendicular to beam direction
Connects centers of colliding nuclei
*Not measured directly* → estimated by centrality

**Centrality**

Determined from *particle multiplicities*

- Most central: 0-5% centrality 
- Peripheral: 70-80% centrality 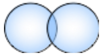

# Event shape engineering

Select events with similar centralities and different shapes based on the event-by-event flow/eccentricity fluctuations

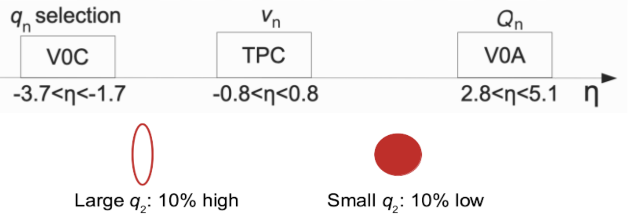


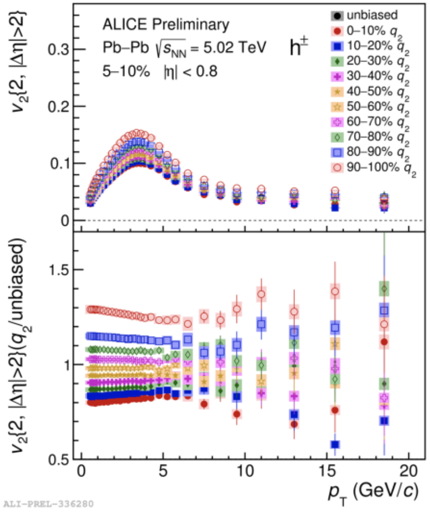

# Event shape engineering

Select events with similar centralities and different shapes based on the event-by-event flow/eccentricity fluctuations

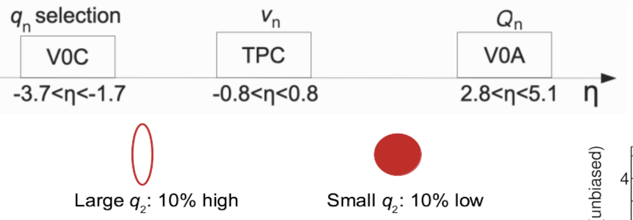


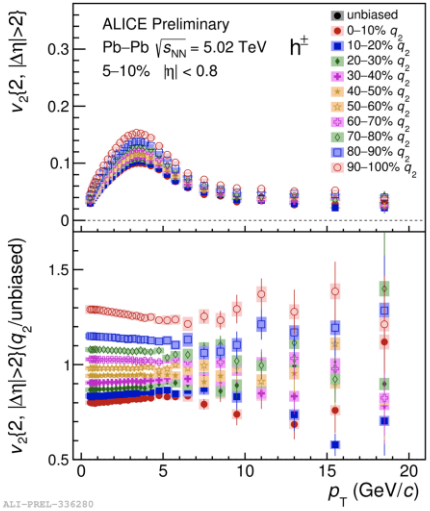


ALICE, PLB 813 (2021) 136054

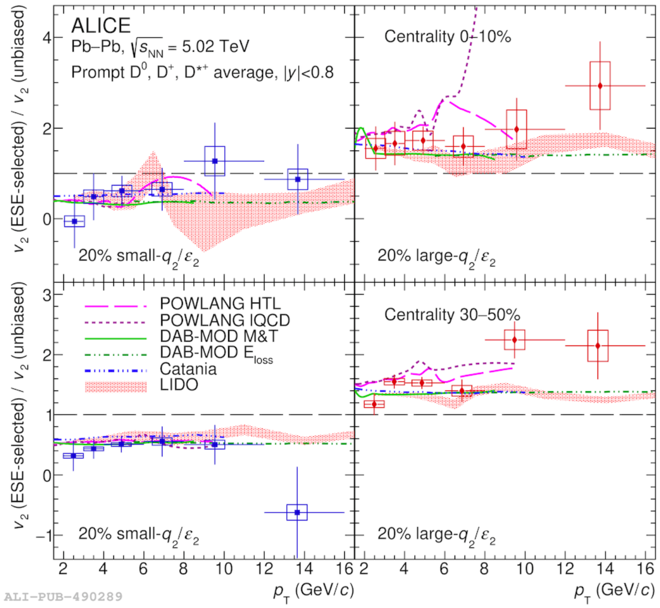


D mesons are sensitive to the light-hadron bulk collectivity and event-by-event fluctuations in the initial stage

# Event shape engineering

Select events with similar centralities and different shapes based on the event-by-event flow/eccentricity fluctuations

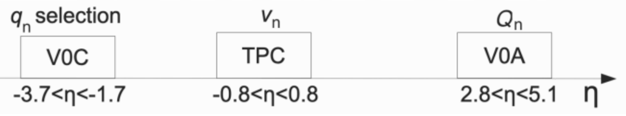


Large $q_2$: 10% high

Small $q_2$: 10% low

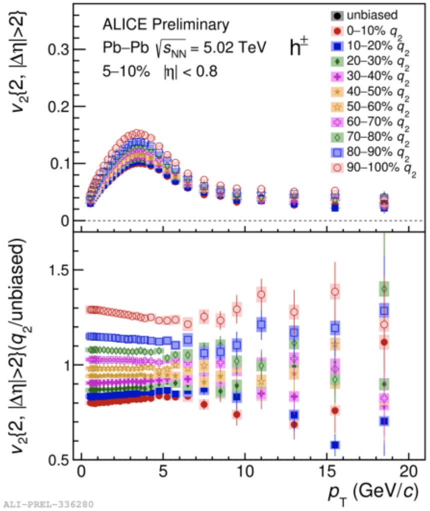


ALICE, PLB 813 (2021) 136054

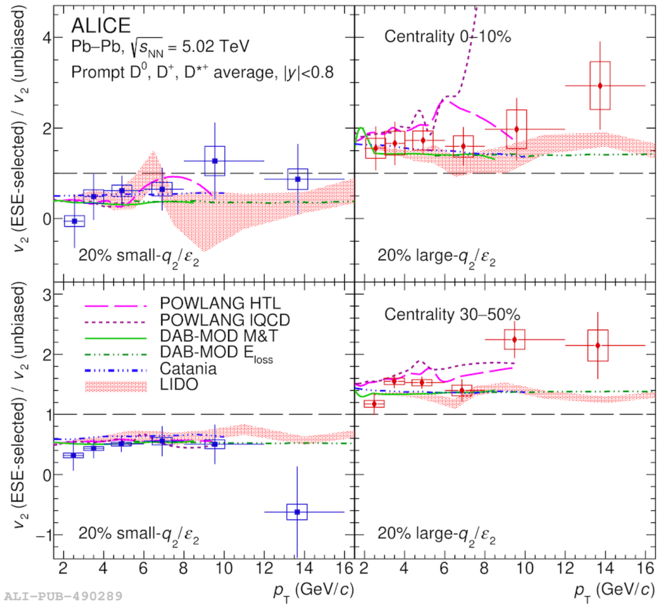


D mesons are sensitive to the light-hadron bulk collectivity and event-by-event fluctuations in the initial stage

ALICE, JHEP 02 (2019) 012

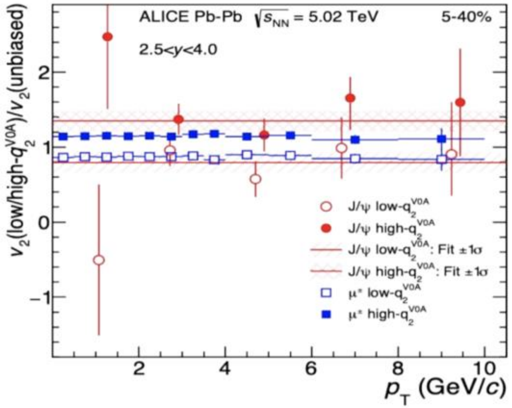


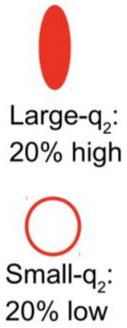


Ratio (ESE/unbiased) of J/Ψ $v_2$ consistent with those of single muons within uncertainties

→ J/Ψ $v_2$ compatible with the expected variations of the initial geometry

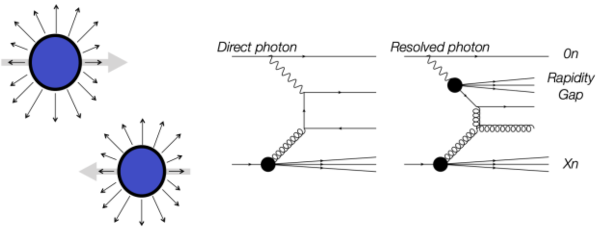


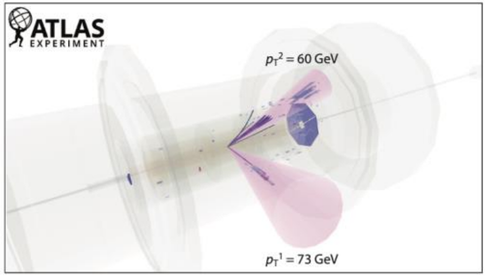


Run: 286717
Event: 36935568
2015-11-26 09:36:37 CEST
Pb+Pb $\sqrt{s_{NN}} = 5.02$ TeV

HION-2015-001

$$H_T \equiv \sum_i p_T^i$$

$$x_A \equiv \frac{M_{jets} e^{-y_{jets}}}{\sqrt{s_{NN}}}$$

$$z_\gamma \equiv \frac{M_{jets} e^{+y_{jets}}}{\sqrt{s_{NN}}}$$

At intermediate photon energies, we can access higher-x partons
Going higher in photon energy opens up the low-x shadowing region

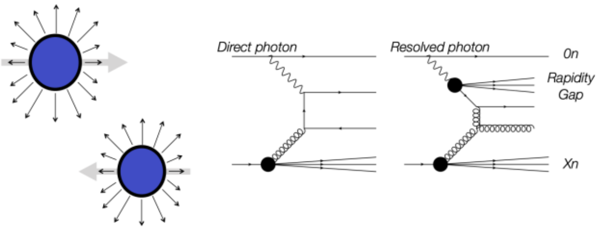


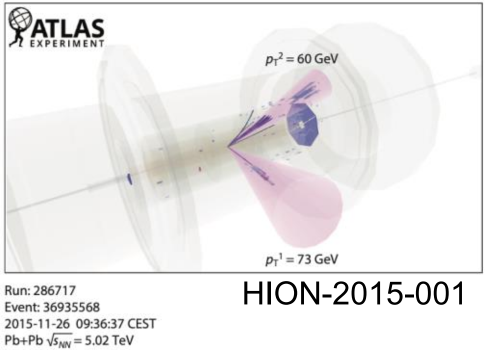


HION-2015-001

$$H_T \equiv \sum_i p_T^i$$

$$x_A \equiv \frac{M_{jets} e^{-y_{jets}}}{\sqrt{s_{NN}}}$$

$$z_\gamma \equiv \frac{M_{jets} e^{+y_{jets}}}{\sqrt{s_{NN}}}$$

ATLAS-CONF-2022-021

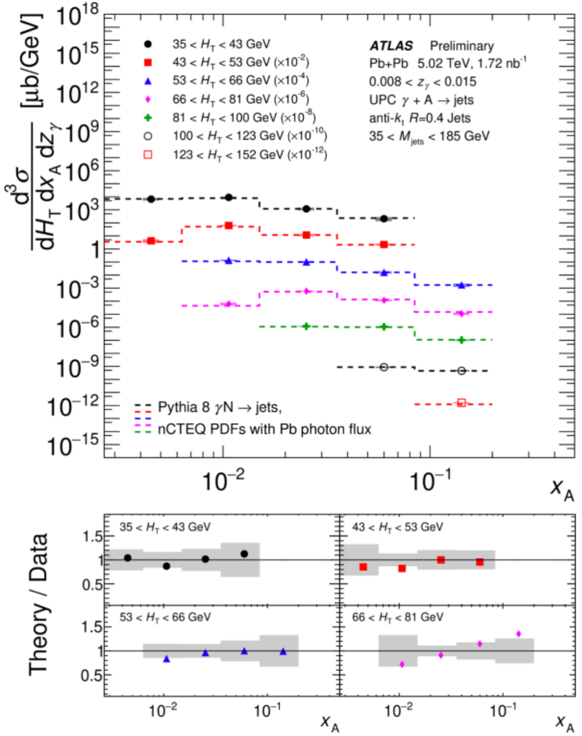


At intermediate photon energies, we can access higher-x partons

Going higher in photon energy opens up the low-x shadowing region

**Results are consistent with theoretical calculations**

# UPC: probing nPDF through photo-nuclear dijet production

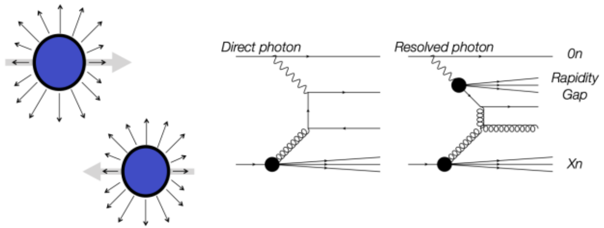


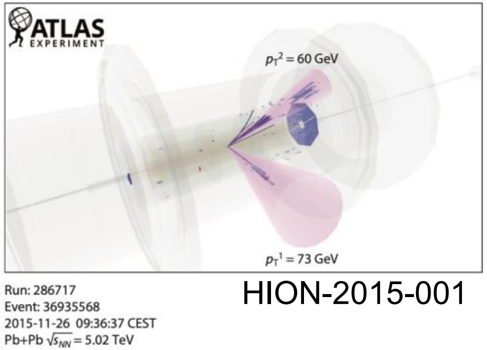


HION-2015-001

$$H_T \equiv \sum_i p_T^i$$

$$x_A \equiv \frac{M_{jets} e^{-y_{jets}}}{\sqrt{s_{NN}}}$$

$$z_\gamma \equiv \frac{M_{jets} e^{+y_{jets}}}{\sqrt{s_{NN}}}$$

ATLAS-CONF-2022-021

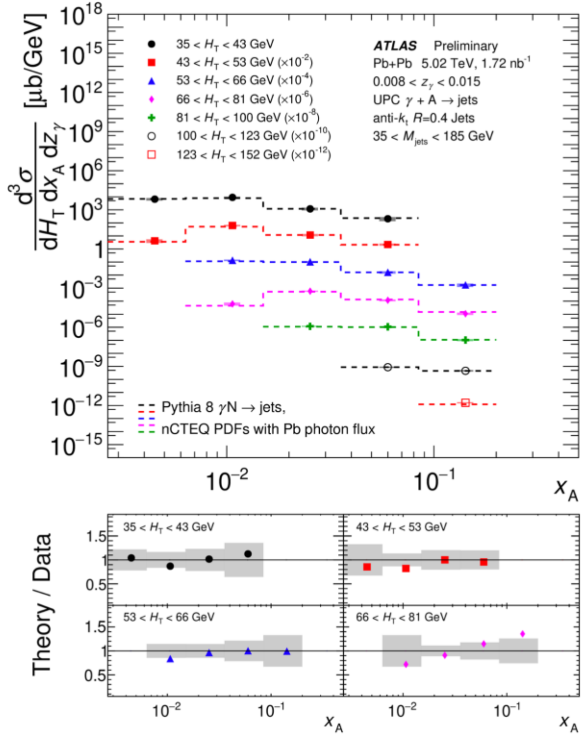


CMS, arXiv:2205.00045

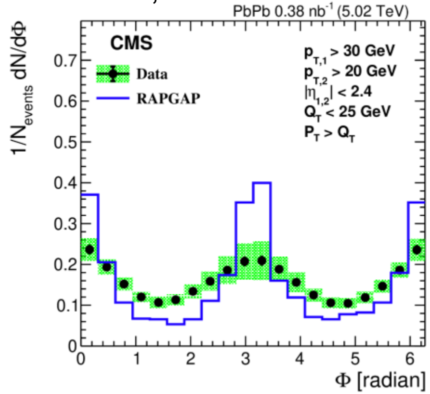


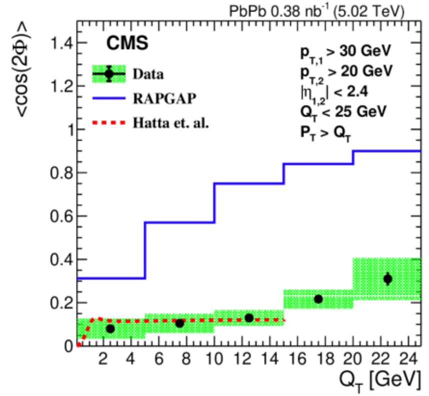


At intermediate photon energies, we can access higher-x partons
Going higher in photon energy opens up the low-x shadowing region
**Results are consistent with theoretical calculations**

Dijet azimuthal angular correlations
→ gluon polarisation in nuclear targets

# Investigating the initial stages with correlations

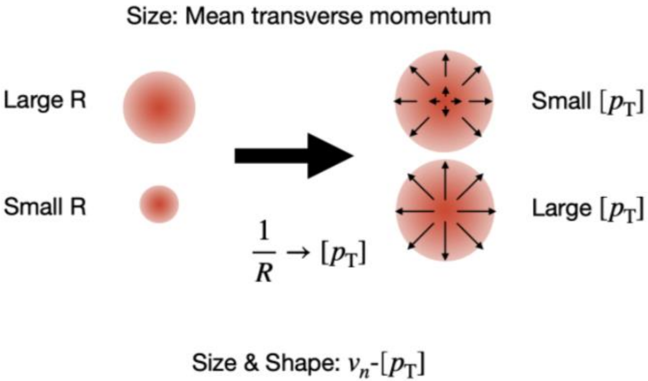


$$\rho(v_n^2, [p_T]) = \frac{cov(v_n^2, [p_T])}{\sqrt{var(v_n^2)}\sqrt{var([p_T])}}$$

ALICE, Phys. Lett. B 834 (2022) 137393

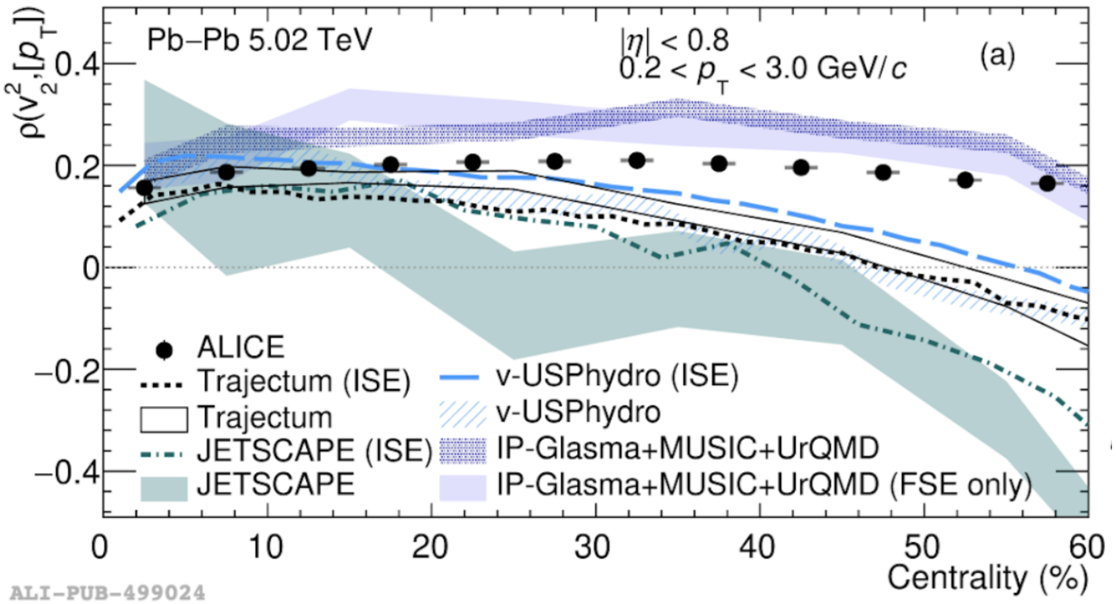


Study of the correlation between the shape of the fireball ($v_2$) and its size ($[p_T]$)

Access to the initial conditions through bulk observables

No quantitative description of the data

Slightly better agreement with models using IP-Glasma initial conditions

# Accessing nuclear deformation through $v_n$-$p_T$ correlation

$v_n$-$p_T$ correlation ($\rho_n$) in initial state between size and eccentricities

PRL 128 (2022) 8, 082301

Sensitive to nuclear geometry

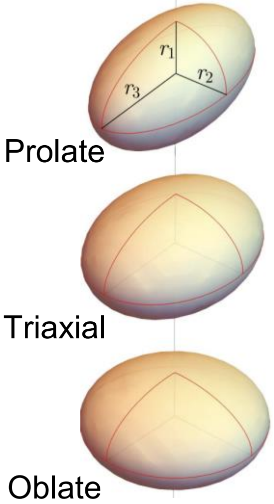


ATLAS-CONF-2021-001

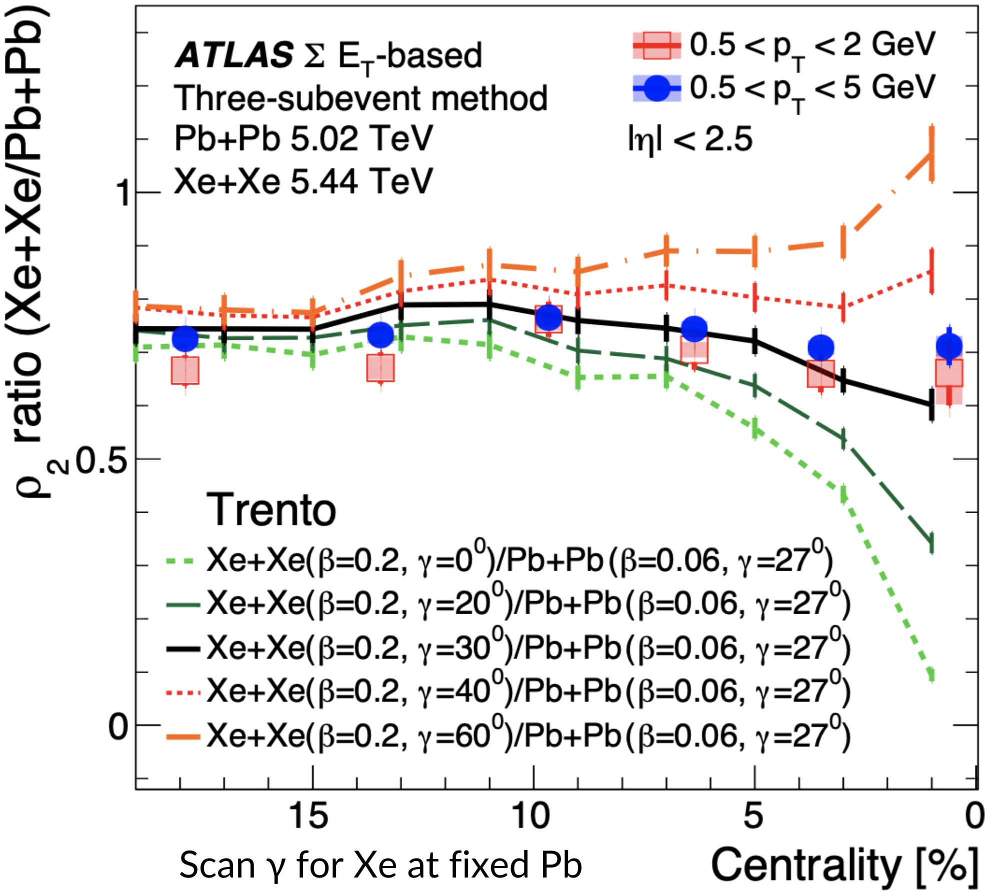


Scan γ for Xe at fixed Pb

Ratio of $\rho_2$ in Xe-Xe and Pb-Pb to take out the final state dependencies

Trento (initial state only) shows large sensitivity to γ of deformed nucleus in central collisions events (where it matters)

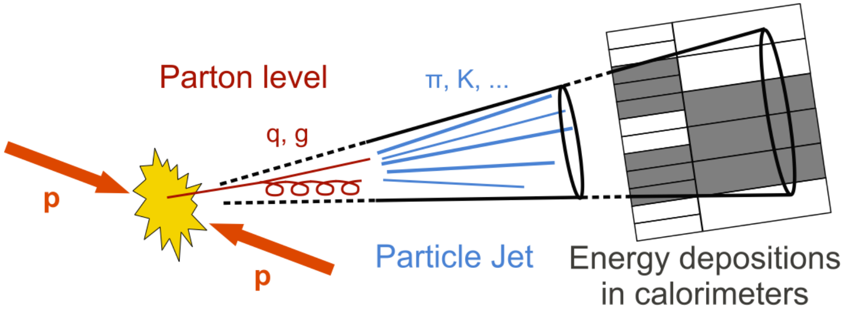


Modification of jets as a probe of quark-gluon plasma

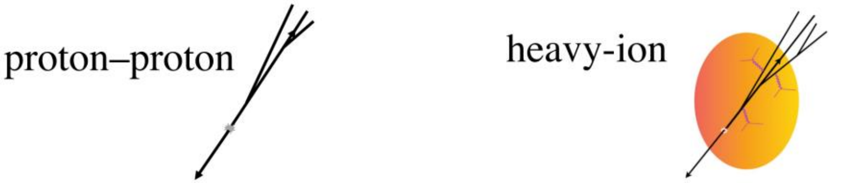


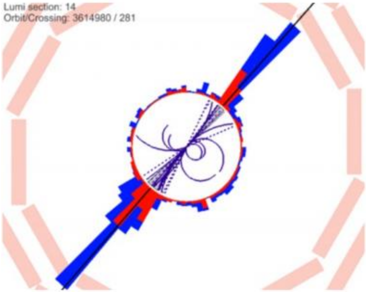

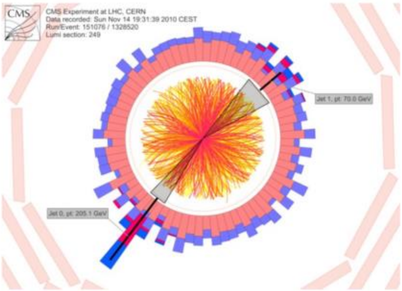

"baseline" jet properties

- Jet: high-$p_T$ parton (quark, gluon) produced at early stage of the collision
- Jet: a collimated spray of particles produced by a high-$p_T$ parton
- Informs about the medium properties due to parton energy loss (jet quenching)

$$\Delta E_{\text{gluon}} > \Delta E_{\text{light quarks}} > \Delta E_{\text{heavy quarks}}$$

ATLAS, PLB 790 (2019) 108

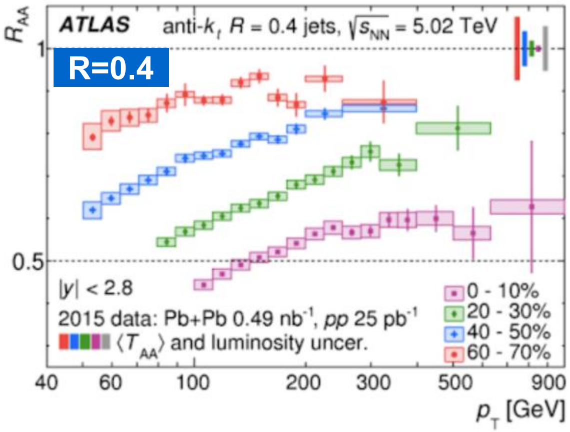


$R_{AA}$ increases with jet $p_T$ reaching a value of about 0.6 at $p_T$ = 1 TeV in central Pb-Pb collisions for R=0.4

R↑ Energy loss recovered within jet "cone"**?**

# Inclusive jet suppression in medium

ATLAS, PLB 790 (2019) 108

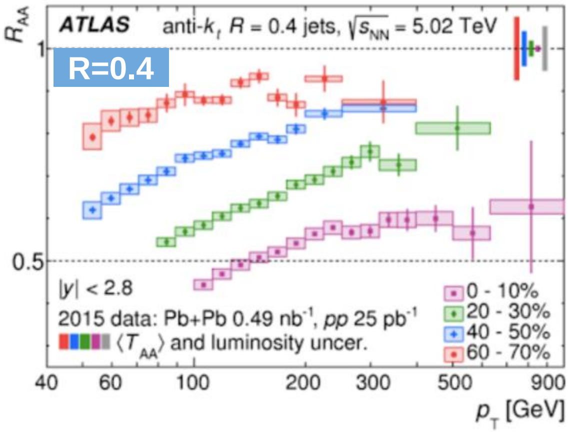


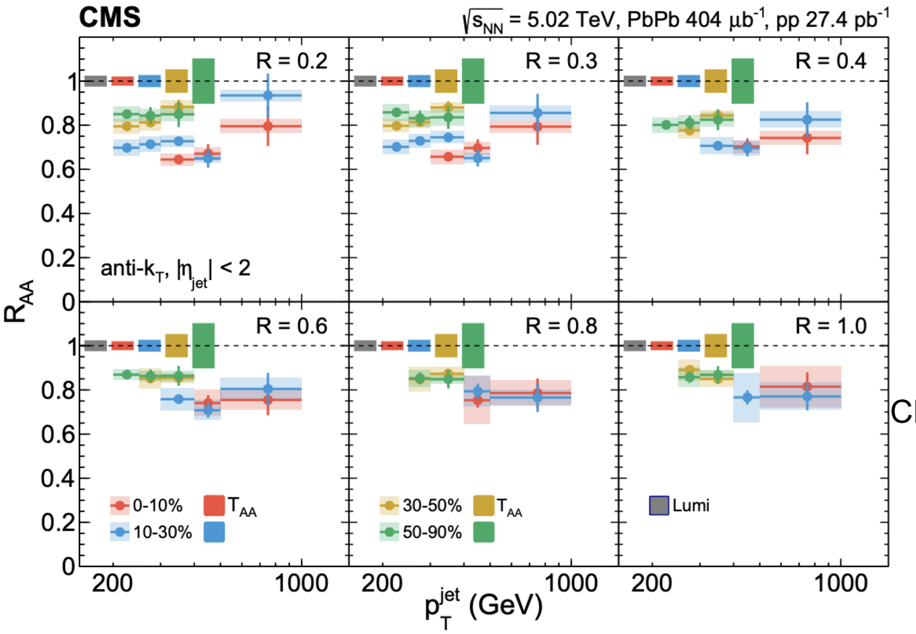


CMS, JHEP 05 (2021) 284

Jet $R_{AA}$ in Pb-Pb collisions shows only a modest increase, $R_{AA}$ never reaches unity

$R_{AA}$ increases with jet $p_T$ reaching a value of about 0.6 at $p_T$ = 1 TeV in central Pb-Pb collisions for R=0.4

R↑ Energy loss recovered within jet "cone"**?**

# Inclusive jet suppression in medium

ATLAS, PLB 790 (2019) 108

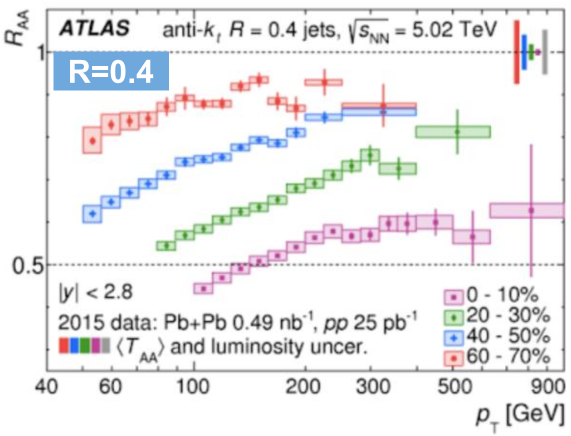


$R_{AA}$ increases with jet $p_T$ reaching a value of about 0.6 at $p_T$ = 1 TeV in central Pb-Pb collisions for R=0.4

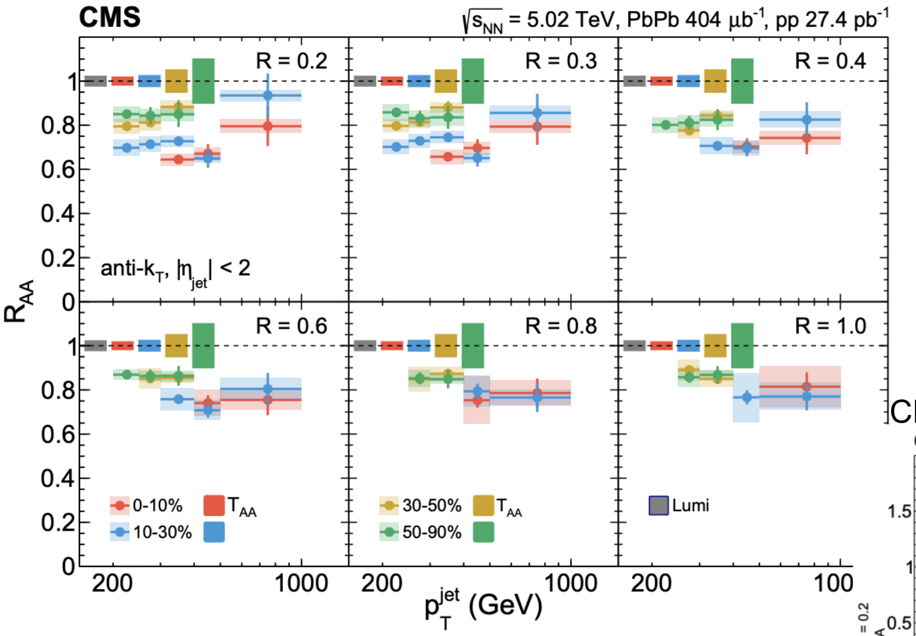


Significant constraints on models of jet quenching, medium response, wide angle radiation

Jet $R_{AA}$ in Pb-Pb collisions shows only a modest increase, $R_{AA}$ never reaches unity

CMS, JHEP 05 (2021) 284

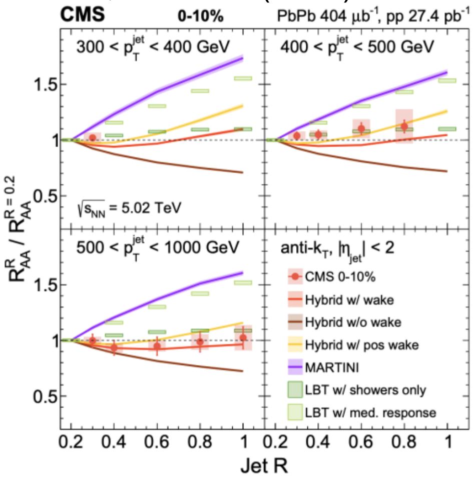


R↑ Energy loss **not** recovered within jet "cone"

**Vacuum**:
Parton shower is a multi-scale process with a given momentum and angular/virtuality scale

**Medium**:
Angular/virtuality scale can be related to a "resolution scale" at which the jet probes the medium

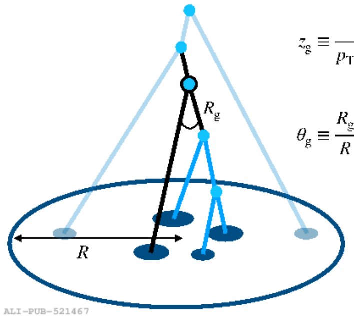


$$z_g \equiv \frac{p_{T,\text{subleading}}}{p_{T,\text{leading}} + p_{T,\text{subleading}}}$$

$$\theta_g \equiv \frac{R_g}{R} \equiv \frac{\sqrt{\Delta y^2 + \Delta\varphi^2}}{R}$$

**Vacuum**:
Parton shower is a multi-scale process with a given momentum and angular/virtuality scale

**Medium**:
Angular/virtuality scale can be related to a "resolution scale" at which the jet probes the medium

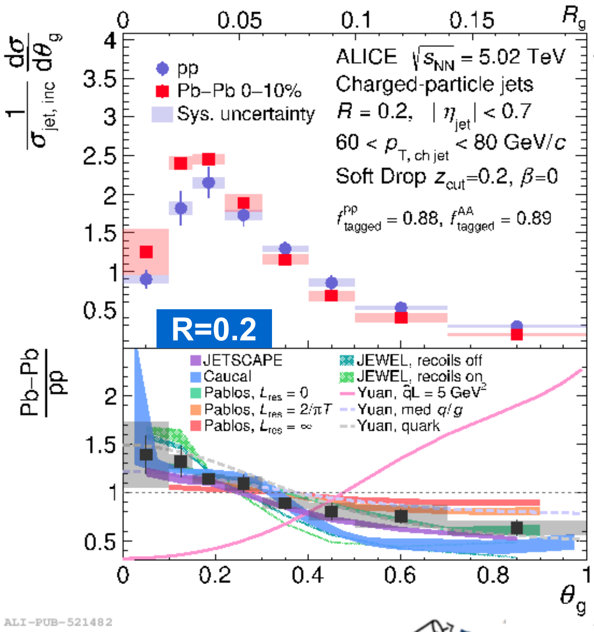


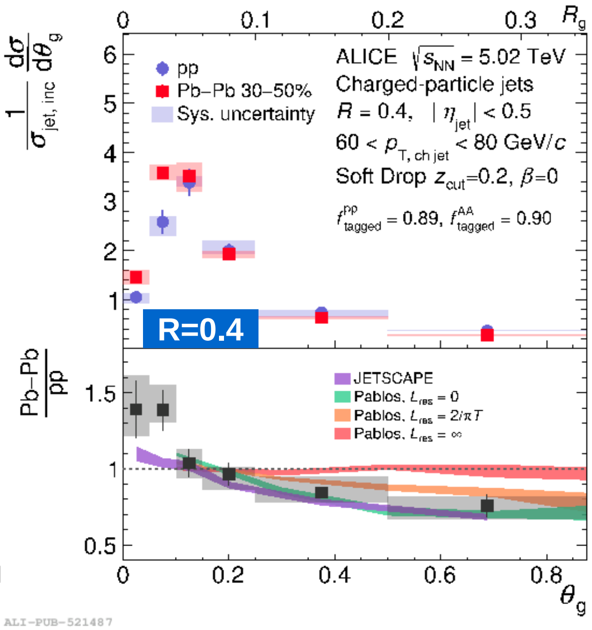


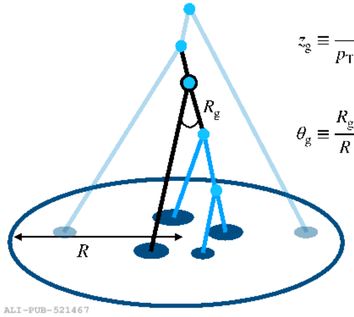


$$z_g \equiv \frac{p_{T,\mathrm{subleading}}}{p_{T,\mathrm{leading}} + p_{T,\mathrm{subleading}}}$$

$$\theta_g \equiv \frac{R_g}{R} \equiv \frac{\sqrt{\Delta y^2 + \Delta\varphi^2}}{R}$$


See also ATLAS-CONF-2022-026

Suppression of large angles and enhancement of small angles. Medium has resolving power for splittings (promotes narrow splittings, filters out wider subjets)

# Color charge dependence of jet energy loss

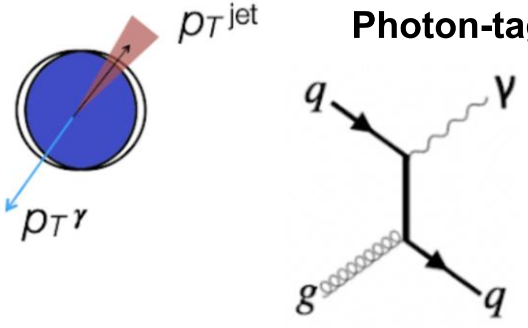


**Photon-tagged jets** → sample dominated by **quark-initiated jets** (quark gluon Compton scattering)

ATLAS-CONF-2022-019

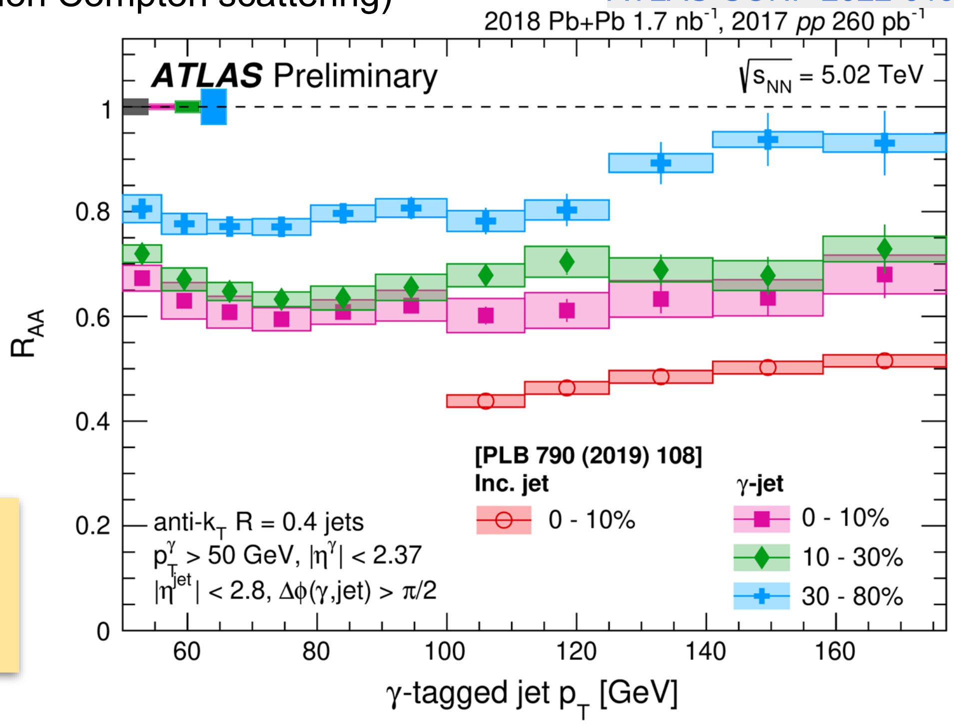


The **photon-tagged jet $R_{AA}$** higher than the **inclusive jet $R_{AA}$**

Clear observation of color factor dependence of Parton-QGP interaction

- Jets recoiling against a high-$p_T$ hadron → down to jet $p_T$ ~ 10 GeV/$c$

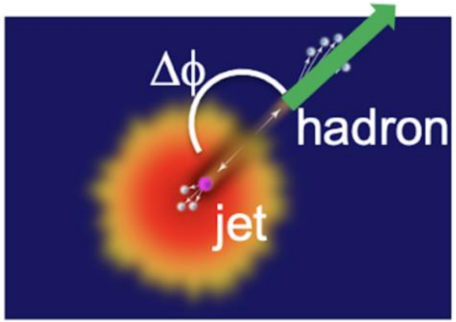


$\Delta_{recoil}$ vs ΔΦ broader in Pb-Pb than in pp

**Angular deflection of soft large-R jets:**
- Scattering on QGP constituents?
- Medium response to energy loss?

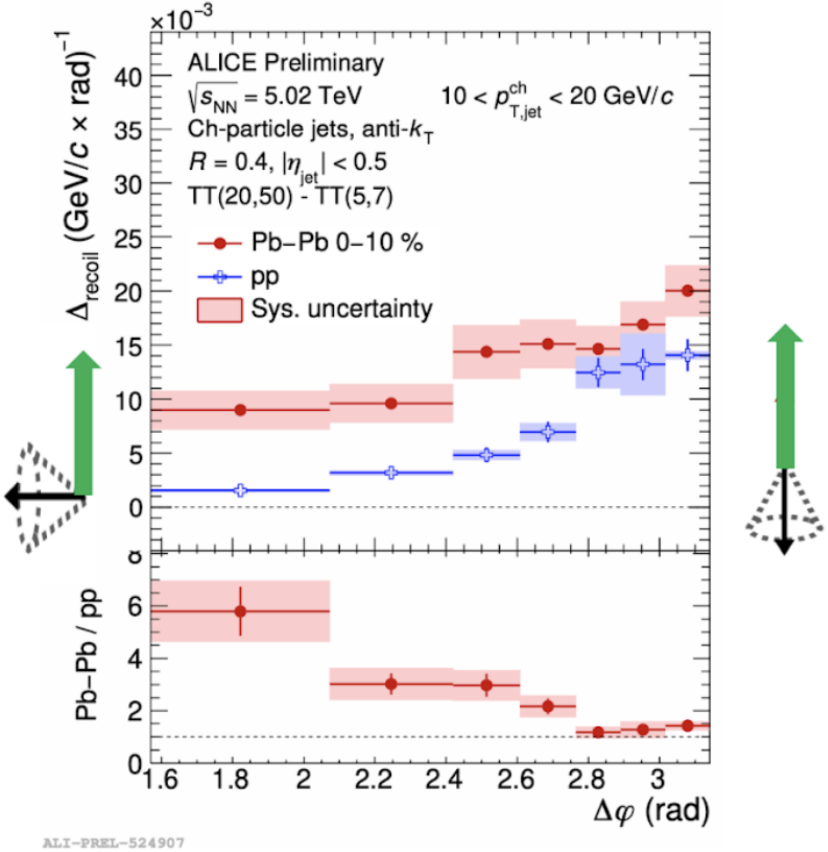

# High precision measurement of jet quenching in p-Pb collisions

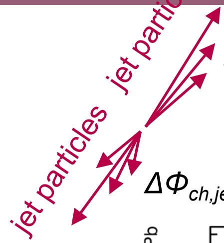


No jet quenching observed in p-Pb despite of collectivity of high-$p_T$ particles

$I_{p\text{-}Pb}$=p-Pb/pp of per-jet yields

arXiv:2206.01138 [nucl-ex]

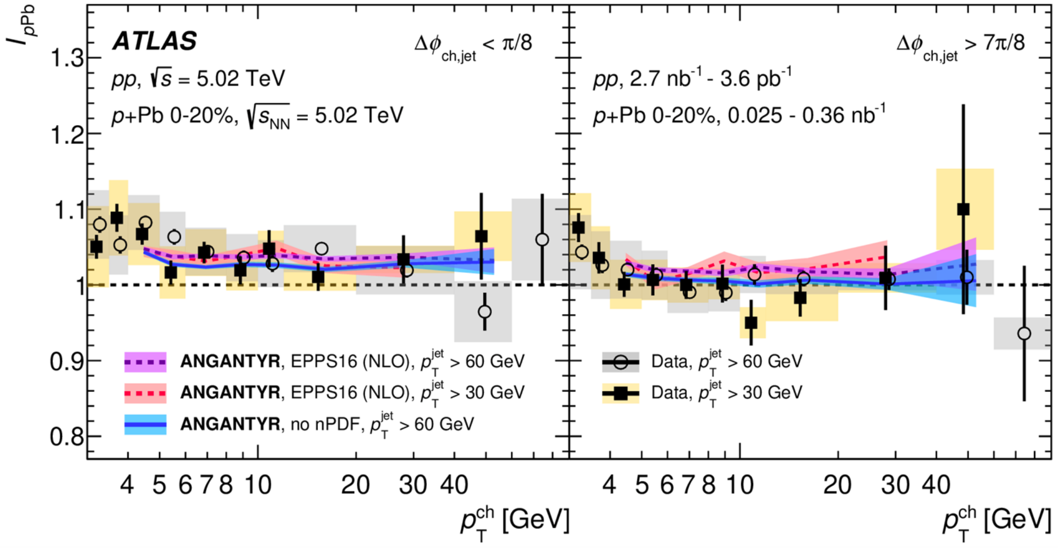


Eur. Phys. J. C80 (2020) 73

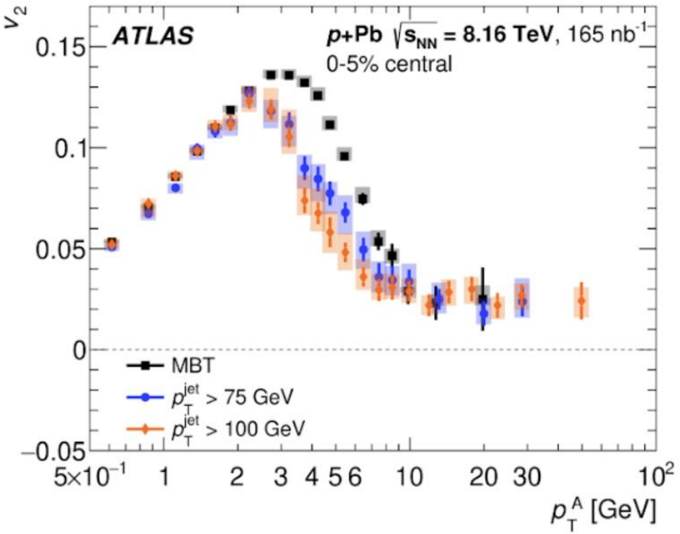


Small to no modifications of hadron yields observed in central p-Pb collisions

- Modification of the jet fragmentation
- Strong constraints on E-loss scenarios

Special run to minimize systematics:
- Fill-by-fill switching
- Level luminosity

$\sqrt{s_{NN}}$ = 200 GeV

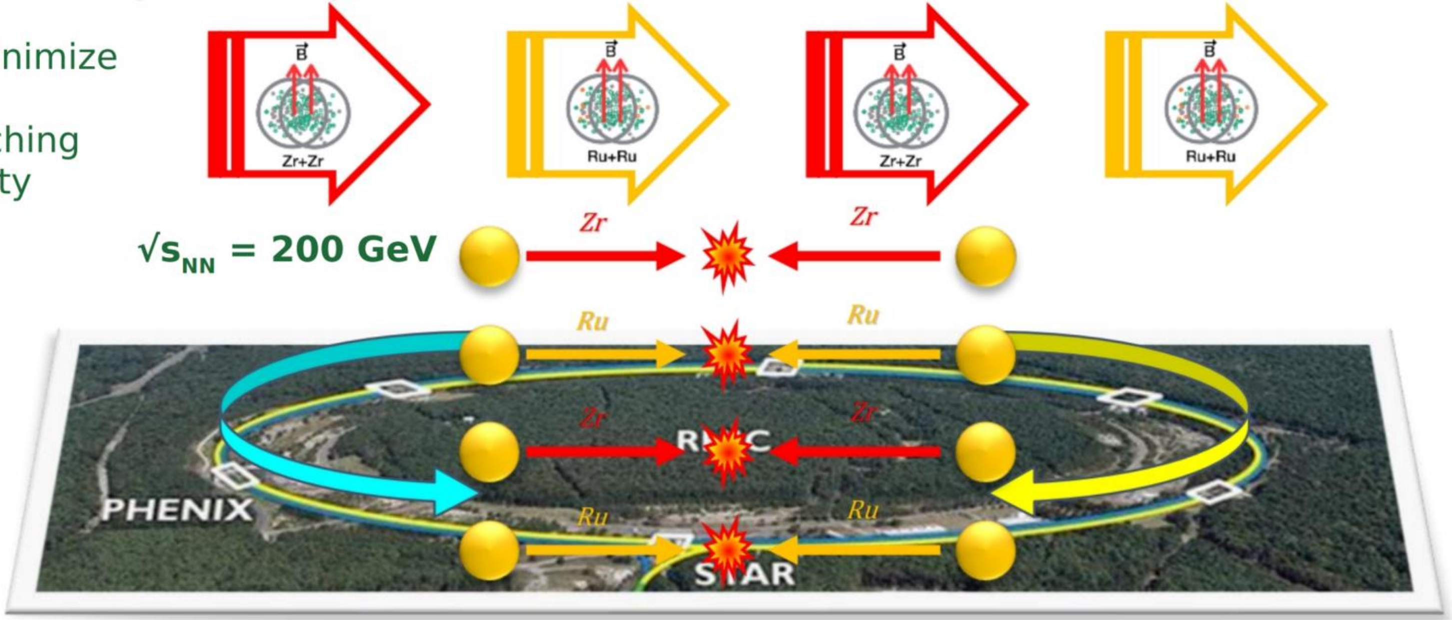

# Details of blind analysis

M. S. Abdallah *et al.* (STAR) Phys. Rev. C, 105 (2022) 014901
J. Adam *et al.* (STAR) Nucl. Sci. Tech. 32 (2021) 48

**STEP-0**
**Mock Data challenge**
Test data structure
(Au+Au data)
~2 months

→

**STEP-1**
**Isobar Mixed Analysis**
Code freezing
(Each run is Ru+Ru & Zr+Zr)
~1 year

→

**STEP-2**
**Isobar Blind analysis**
QA with ~ 1% data
(Each run is Ru+Ru or Zr+Zr)
~1/2 year

→

**STEP-3**
**Isobar Unblind analysis**
Final analysis
(Ru+Ru & Zr+Zr separated)
~2-3 months

**Blind analyses (5 groups):**

- ❖ $\Delta\gamma, \Delta\delta$ *and* κ
- ❖ $\Delta\gamma, \Delta\delta, \Delta\gamma(\Delta\eta)$
- ❖ $\Delta\gamma$ *in* PP/SP , $\Delta\gamma(M_{inv})$
- ❖ $\Delta\gamma$ *in* PP/SP
- ❖ $R(\Delta S)$ Correlator.

A large, collective effort

Connections between the methods are studied

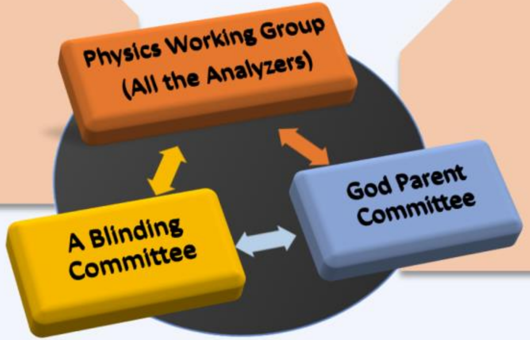


**Using the frozen code from STEP-1:**

- ❖ Sensitivity of observables tested using AVFD simulation
- ❖ Similar sensitivities are found in all observables

S. Choudhury *et al.* Chin. Phys. C, 46 (2022) 014101

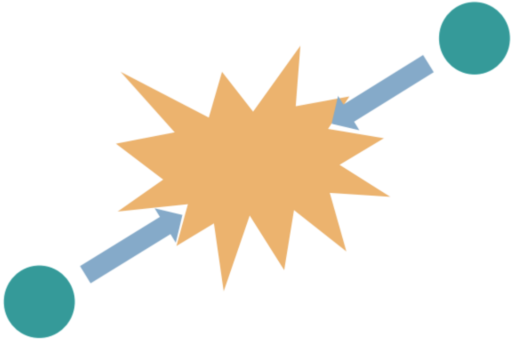

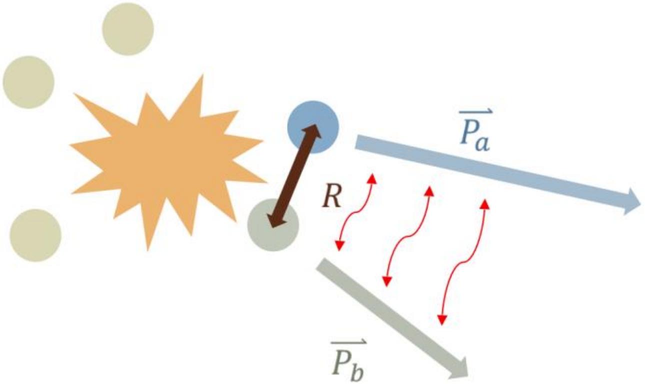


$$k^* = \frac{|\,\boldsymbol{p}_a^* - \boldsymbol{p}_b^*\,|}{2}$$

$$C(k^*) = \frac{P(\overrightarrow{p_a}, \overrightarrow{p_b})}{P(\overrightarrow{p_a})P(\overrightarrow{p_b})} \qquad k^* = \frac{|\,\boldsymbol{p}_a^* - \boldsymbol{p}_b^*\,|}{2}$$

**experiment**

$$C(k^*) = \mathcal{N}\frac{N_{Same}(k^*)}{N_{Mixed}(k^*)}$$

$N_{Same}(k^*)$ - correlated pairs ("same events")

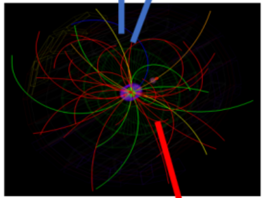

Event 1

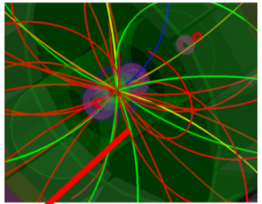

Event 2

$N_{Mixed}(k^*)$ - uncorrelated pairs ("mixed events")

**theory (models)**

c

$$C(k^*) = \int S(r^*) \;\; |\Psi(\boldsymbol{k}^*, \boldsymbol{r}^*)|^2 \, d^3 r^*$$

ALI-PUB-483391

Emission source

Two-particle wave function

$$C(k^*) = \frac{P(\overrightarrow{p_a}, \overrightarrow{p_b})}{P(\overrightarrow{p_a})P(\overrightarrow{p_b})} \qquad k^* = \frac{|\,\boldsymbol{p}_a^* - \boldsymbol{p}_b^*\,|}{2}$$

**experiment**

$$C(k^*) = \mathcal{N}\frac{N_{Same}(k^*)}{N_{Mixed}(k^*)}$$

$N_{Same}(k^*)$ - correlated pairs (“same events”)

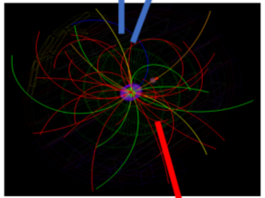

Event 1

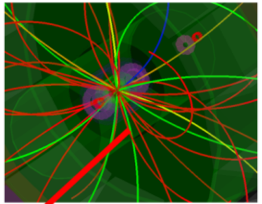

Event 2

$N_{Mixed}(k^*)$ - uncorrelated pairs (“mixed events”)

**theory (models)**

c

$$C(k^*) = \int \; S(r^*) \;\; |\Psi(\boldsymbol{k}^*, \boldsymbol{r}^*)|^2 \, d^3 r^*$$

ALI-PUB-483391

Emission source

Two-particle

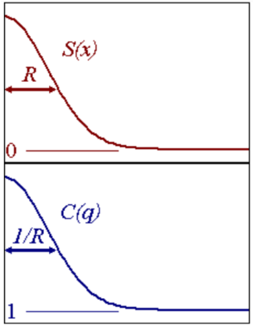


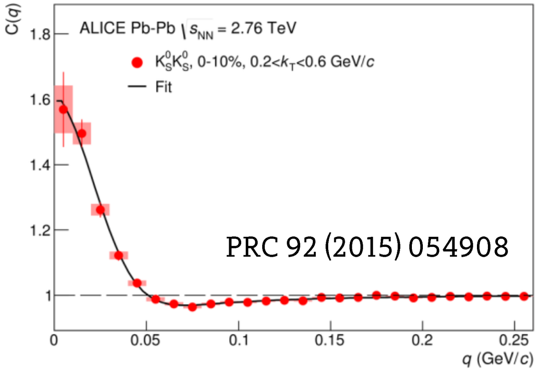

# Femtoscopy measurements

$$C(k^*) = \frac{P(\overrightarrow{p_a}, \overrightarrow{p_b})}{P(\overrightarrow{p_a})P(\overrightarrow{p_b})}$$

$$k^* = \frac{|\, \boldsymbol{p}_a^* - \boldsymbol{p}_b^* \,|}{2}$$

## experiment

$$C(k^*) = \mathcal{N} \frac{N_{Same}(k^*)}{N_{Mixed}(k^*)}$$

$N_{Same}(k^*)$ - correlated pairs (“same events”)

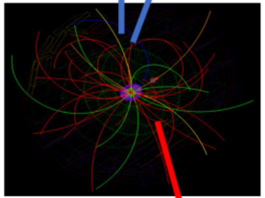

Event 1

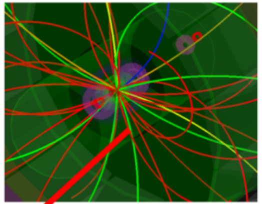

Event 2

$N_{Mixed}(k^*)$ - uncorrelated pairs (“mixed events”)

## theory (models)

c

$$C(k^*) = \int \; S(r^*) \;\; |\Psi(\boldsymbol{k}^*, \boldsymbol{r}^*)|^2 \, d^3 r^*$$

ALI-PUB-483391

Emission source

Two-particle wave function

$$m_T = \sqrt{k_T^2 + m_0^2}$$

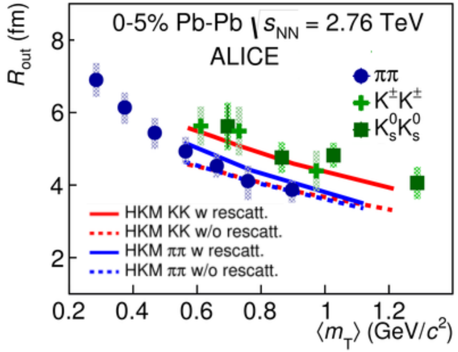

# Femtoscopy measurements – source size

PLB 813 (2021) 136030

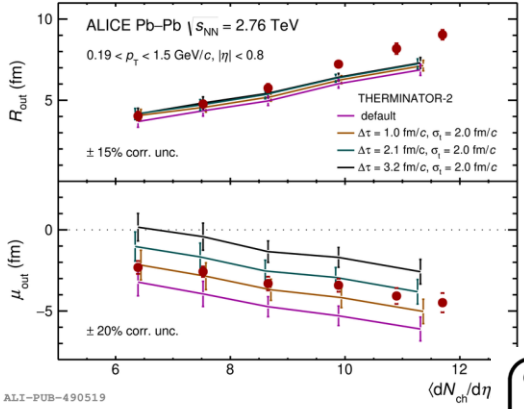


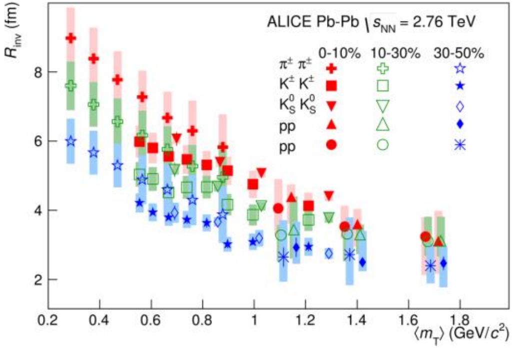


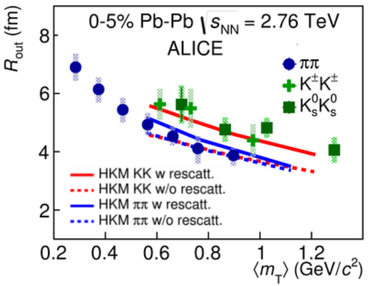


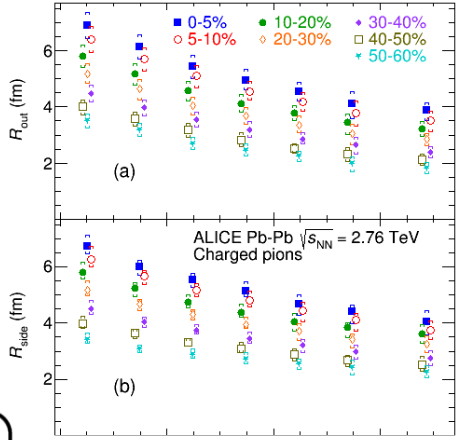


Phys. Rev. C93 (2016) 024905

$$C(k^*) = \int S(r^*) \; |\Psi(\boldsymbol{k}^*, \boldsymbol{r}^*)|^2 \, d^3r^* = \xi(k^*) \cdot \frac{N_{\mathrm{same}}(k^*)}{N_{\mathrm{mixed}}(k^*)}$$

Phys. Lett. B 811 (2020) 135849
arXiv:2004.08018

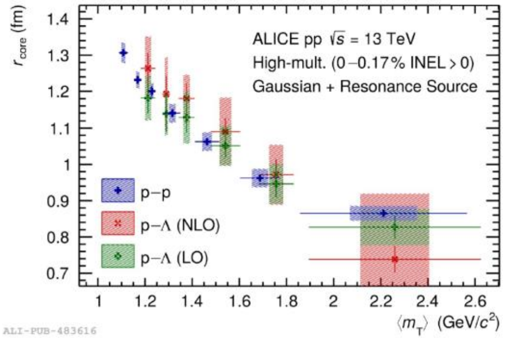


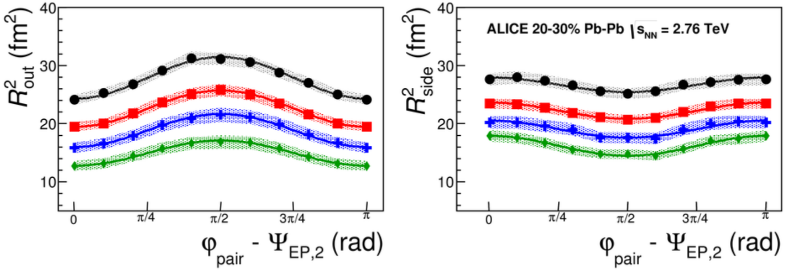


Phys. Rev. Lett. 118 (2017) 222301

arXiv:2111.06611

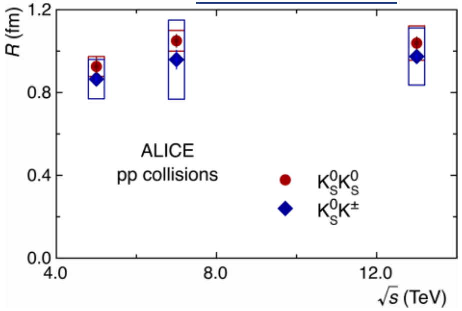

**Femtoscopic correlation function** carry information about the particle source $S(r^*)$ from which pairs emerge, as well as the interaction potential via the two-particle wave function ***ψ*(*k**,*r**)**.

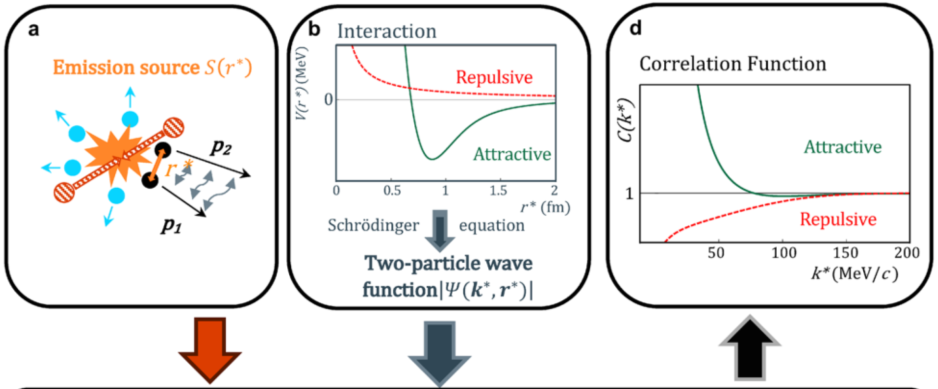


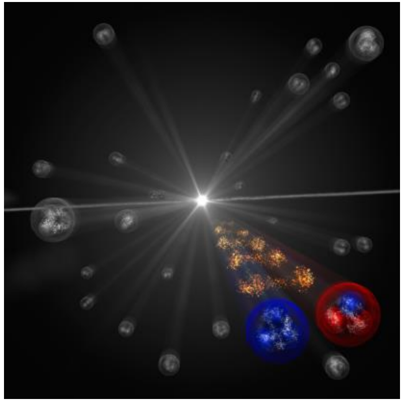

c

measured known unknown

$$C(k^*) = \int S(r^*)\,|\Psi(\boldsymbol{k}^*, \boldsymbol{r}^*)|^2\, d^3r^* = \xi(k^*) \cdot \frac{N_{\mathrm{same}}(k^*)}{N_{\mathrm{mixed}}(k^*)}$$

ALI−PUB−483391

- We constrain the source $S(r^*)$ from pairs where interaction is known
- We can use femtoscopy to measure the interactions ***ψ*** between other particle species

# Why study interactions?

u d content — s c b content

Scattering experiments

Exotic atoms and hypernuclei

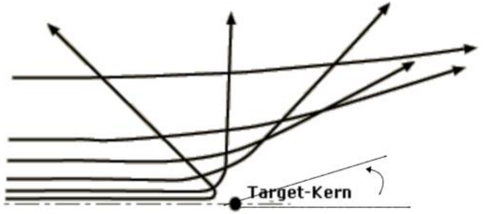


$$\longrightarrow \quad \frac{d\sigma}{d\Omega}$$

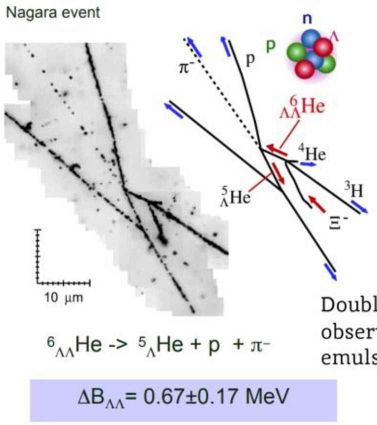


Double-Λ hypernuclei observed in a hybrid emulsion experiment

*H. Takahashi et al., PRL 87 (2001) 212502*

17/43

# Why study interactions?

u d content — s c b content

Scattering experiments

Exotic atoms and hypernuclei

Chiral effective field theories

Lattice QCD

Final State Interactions of hadrons produced in pp, pA and AA collisions

**Correlation analysis**

Exceptional reconstruction and PID capabilities of ALICE

# Femtoscopy measurements – not only LHC!

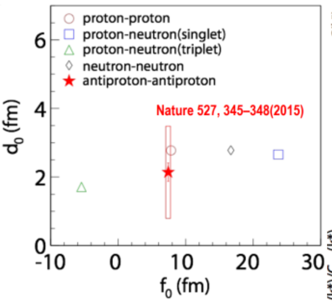


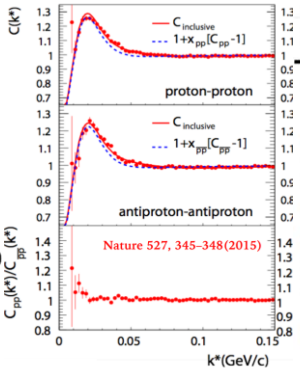


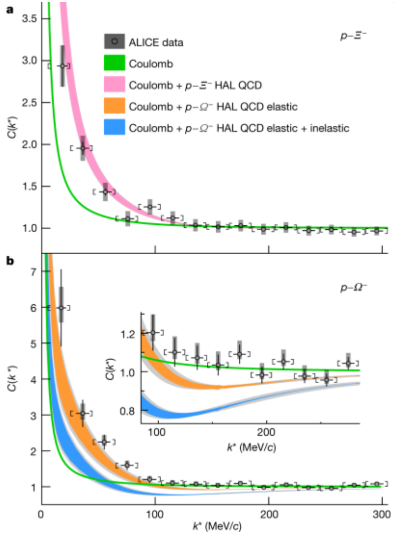


**nature**

Explore content ⌄ About the journal ⌄ Publish with us ⌄ Subscribe

nature > letters > article

Published: 04 November 2015

## Measurement of interaction between antiprotons

The STAR Collaboration

*Nature* **527**, 345–348 (2015) | Cite this article



ℹ This article has been updated

### Abstract

One of the primary goals of nuclear physics is to understand the force between nucleons, which is a necessary step for understanding the structure of nuclei and how nuclei interact with each other. Rutherford discovered the atomic nucleus in 1911, and the large body of knowledge about the nuclear force that has since been acquired was derived from studies made on nucleons or nuclei. Although antinuclei up to antihelium-4 have been discovered[1] and their masses measured, little is known directly about the nuclear force between antinucleons. Here, we study antiproton pair correlations among data collected by the STAR experiment[2] at the Relativistic Heavy Ion Collider (RHIC)[3], where gold ions are collided with a centre-of-mass energy of 200 gigaelectronvolts per nucleon pair. Antiprotons are abundantly produced in such collisions, thus making it feasible to study details of the antiproton–antiproton interaction. By applying a technique similar to Hanbury Brown and Twiss intensity interferometry[4], we show that the force between two antiprotons is attractive. In addition, we report two key parameters that characterize the corresponding strong interaction: the scattering length and the effective range of the interaction. Our measured parameters are consistent within errors with the corresponding values for proton–proton interactions. Our results provide direct information on the interaction between two antiprotons, one of the simplest systems of antinucleons, and so are fundamental to understanding the structure of more-complex antinuclei and their properties.

**nature**

Explore content ⌄ About the journal ⌄ Publish with us ⌄

nature > articles > article

Article | Open Access | Published: 09 December 2020

## Unveiling the strong interaction among hadrons at the LHC

ALICE Collaboration

*Nature* **588**, 232–238 (2020) | Cite this article



ℹ A Publisher Correction to this article was published on 15 January 2021

ℹ This article has been updated

### Abstract

One of the key challenges for nuclear physics today is to understand from first principles the effective interaction between hadrons with different quark content. First successes have been achieved using techniques that solve the dynamics of quarks and gluons on discrete space-time lattices[1,2]. Experimentally, the dynamics of the strong interaction have been studied by scattering hadrons off each other. Such scattering experiments are difficult or impossible for unstable hadrons[3,4,5,6] and so high-quality measurements exist only for hadrons containing up and down quarks[7]. Here we demonstrate that measuring correlations in the momentum space between hadron pairs[8,9,10,11,12] produced in ultrarelativistic proton–proton collisions at the CERN Large Hadron Collider (LHC) provides a precise method with which to obtain the missing information on the interaction dynamics between any pair of unstable hadrons. Specifically, we discuss the case of the interaction of baryons containing strange quarks (hyperons). We demonstrate how, using precision measurements of proton–omega baryon correlations, the effect of the strong interaction for this hadron–hadron pair can be studied with precision similar to, and compared with, predictions from lattice calculations[13,14]. The large number of hyperons identified in proton–proton collisions at the LHC, together with accurate modelling[15] of the small (approximately one femtometre) inter-particle distance and exact predictions for the correlation functions, enables a detailed determination of the short-range part of the nucleon-hyperon interaction.

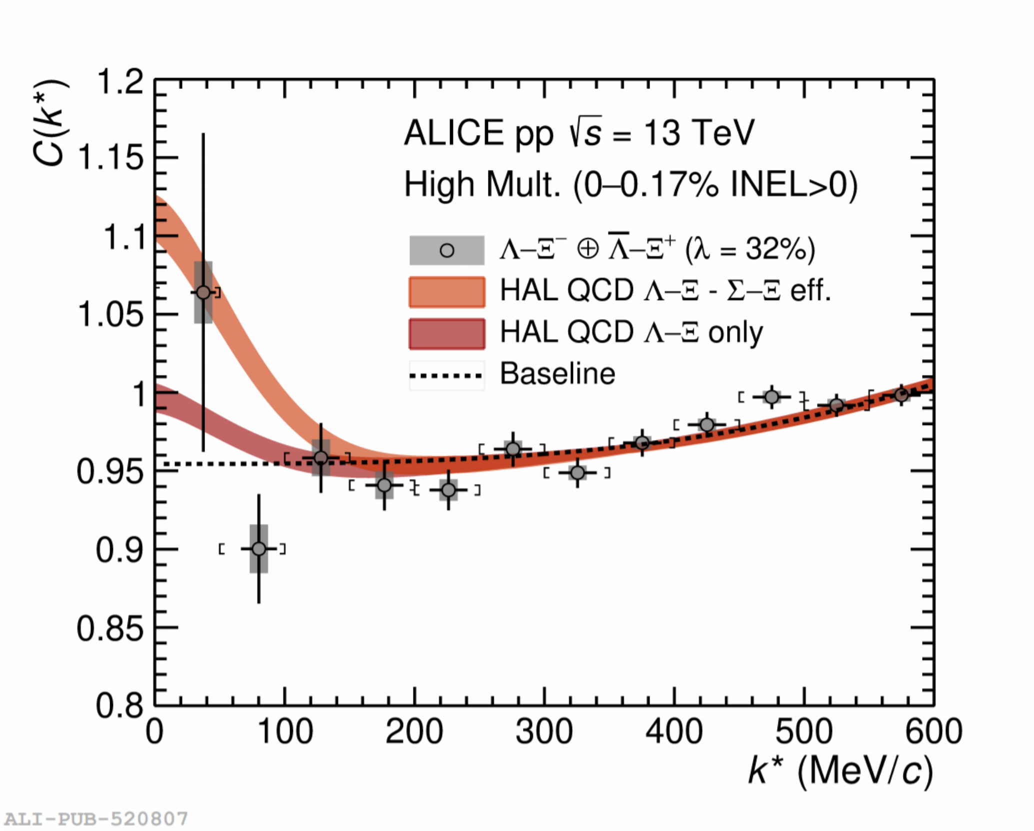


arXiv:2204.10258

First measurement of the ΛΞ-interaction :

- three units of strangeness,
- constraints for lattice QCD calculations and chiral potentials,
- more precision needed.

# D-meson and light hadrons interactions

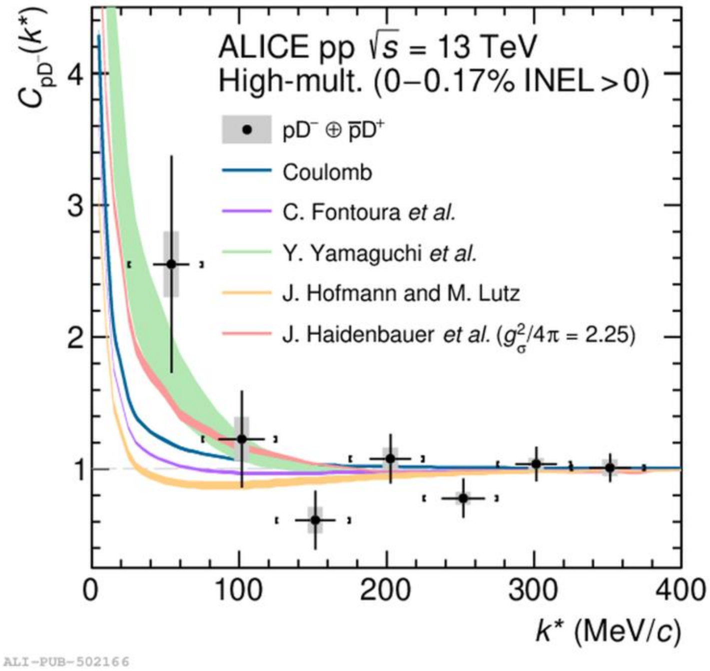


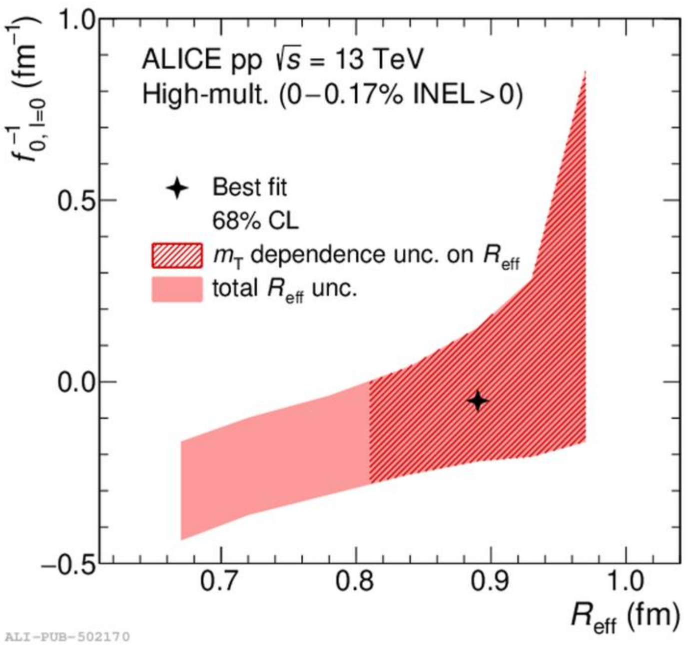


- First measurement of the charm-proton correlation function.
- Coulomb - baseline production, with models including attractive and repulsive interaction.

- Shallow interaction between charm mesons and nucleons
- We extracted with one sigma uncertainty confidence level value of scattering length - Formation of a bound state is not excluded!

# D-meson and light hadrons interactions

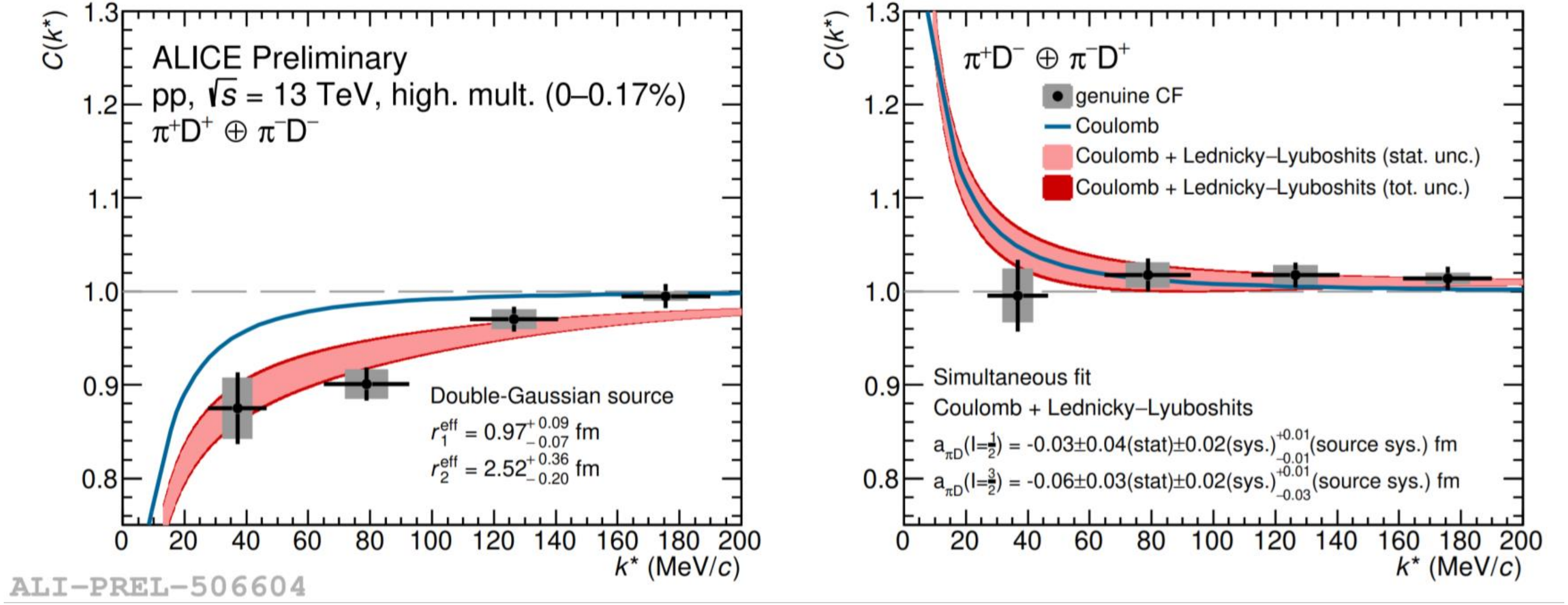


- First studies show a shallow interaction between D mesons and light mesons

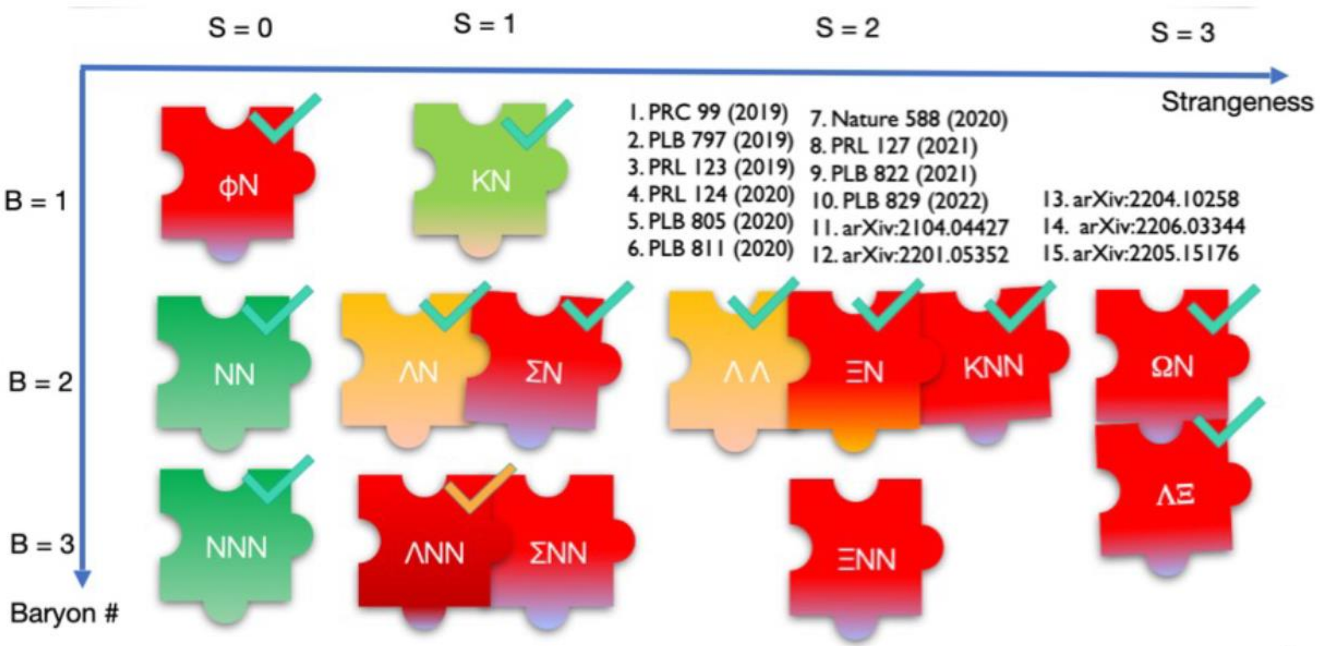
S = 0
S = 1
S = 2
S = 3
Strangeness
B = 1
B = 2
B = 3
Baryon #
ϕN
KN
NN
ΛN
ΣN
Λ Λ
ΞN
KNN
ΩN
ΛΞ
NNN
ΛNN
ΣNN
ΞNN
1. PRC 99 (2019)
2. PLB 797 (2019)
3. PRL 123 (2019)
4. PRL 124 (2020)
5. PLB 805 (2020)
6. PLB 811 (2020)
7. Nature 588 (2020)
8. PRL 127 (2021)
9. PLB 822 (2021)
10. PLB 829 (2022)
11. arXiv:2104.04427
12. arXiv:2201.05352
13. arXiv:2204.10258
14. arXiv:2206.03344
15. arXiv:2205.15176

# Scattering parameters

$$C(q)=\int S(r)|\Psi(q,r)|^2 d^4 r$$

measured correlation

emission function (source size/shape)

pair wave function (includes cross section)

pair wave function $\longrightarrow$ $\Psi=\exp(-ik^* r)+f\frac{\exp(ik^* r)}{r}$

scattering amplitude $\longrightarrow$ $f^{-1}(k^*)=\frac{1}{f_0}+\frac{1}{2}d_0 k^{*2}-ik^*$

Approximate solution

## Correlation function:

$$C(k^*)=1+\sum_S \rho_S\left[\frac{1}{2}\left|\frac{f^S(k^*)}{R}\right|^2\left(1-\frac{d_0^S}{2\sqrt{\pi}R}\right)+\frac{2\Re f^S(k^*)}{\sqrt{\pi}R}F_1(2k^*R)-\frac{\Im f^S(k^*)}{R}F_2(2k^*R)\right]$$

**$f_0$** and **$d_0$** - two important parameters of strong interaction between two particles:

- **$d_0$** - effective range of strong interaction between two particles; it corresponds to the range of the potential in an simplified scenario - the square well potential.
- **$f_0$** - scattering length, determines low-energy scattering (complex number)

Elastic cross section (at low k*) is determined by the scattering length: $\lim_{k\to 0}\sigma_e = 4\pi f_0^2$

- $d_0$ - effective range of strong interaction between two particles; it corresponds to the range of the potential in an simplified scenario - the square well potential.
- $f_0$ - scattering length, determines low-energy scattering (complex number)

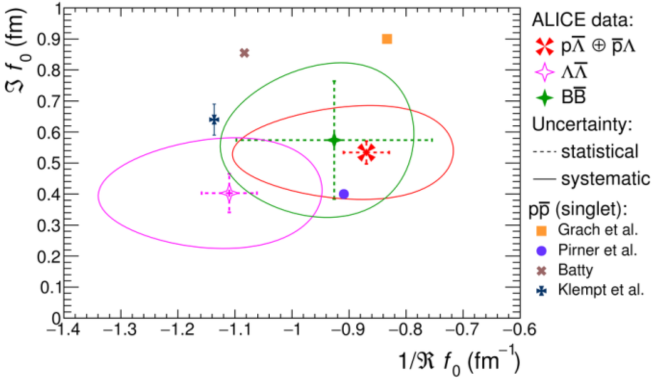


Conclusions from the study:

- Scattering parameters for **all baryon-antibaryon pairs are similar to each other**
- We observe a **negative real part of scattering length** → repulsive strong interaction or creation of a bound state (existence of baryon-antibaryon bound states?)
- Significant **positive imaginary part of scattering length** – presence of a non-elastic channel – annihilation

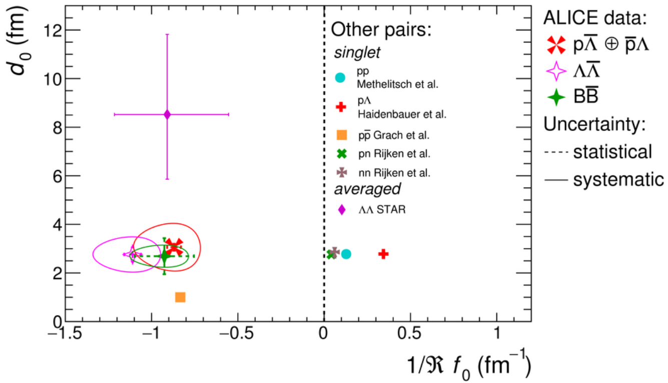


PLB 802 (2020) 135223

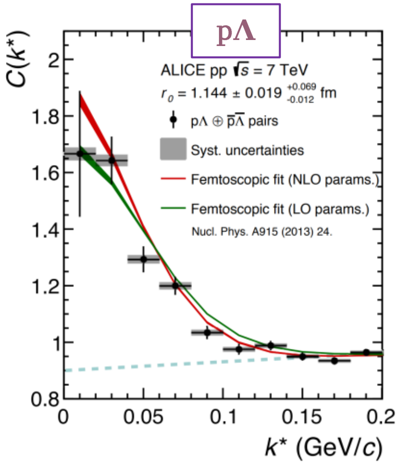


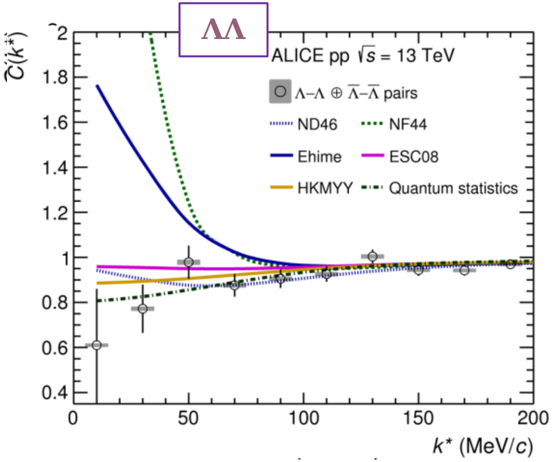


PRC 99 (2019) 024001

For details see CERN-LHC Seminar
25 Sep 2018
https://indico.cern.ch/event/749074/

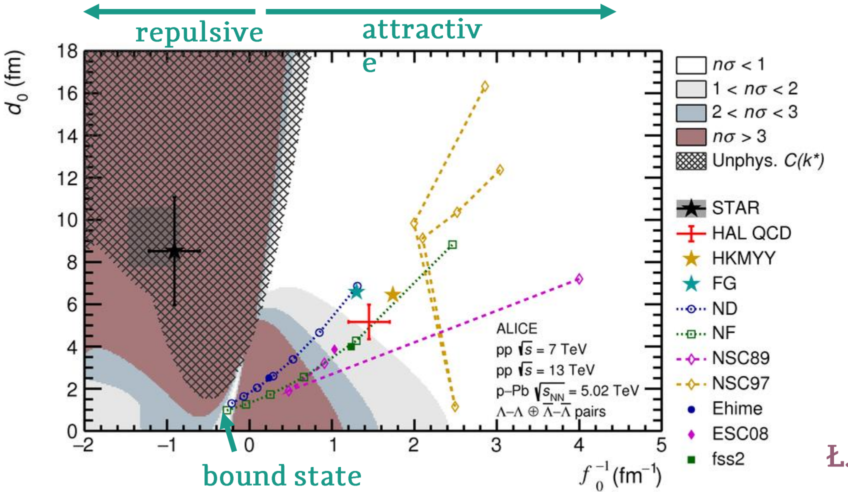


- Interaction of nucleons and different hyperons – constraining neutron stars EoS
- Constraining lambda-lambda scattering parameters and bound states (H-dibaryon)

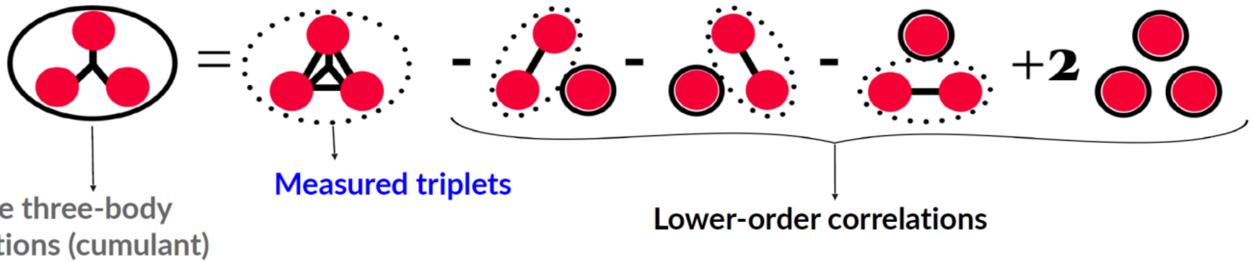


R. Del Grande et al., Eur. Phys. J. C 82, 244 (2022)
arXiv:2107.10227

- ALICE is pioneering new methods to explore the three body interactions
- First measurement of the genuine three-body interactions via cumulants

$$Q_3 = \sqrt{-q_{12}^2 - q_{23}^2 - q_{31}^2}$$

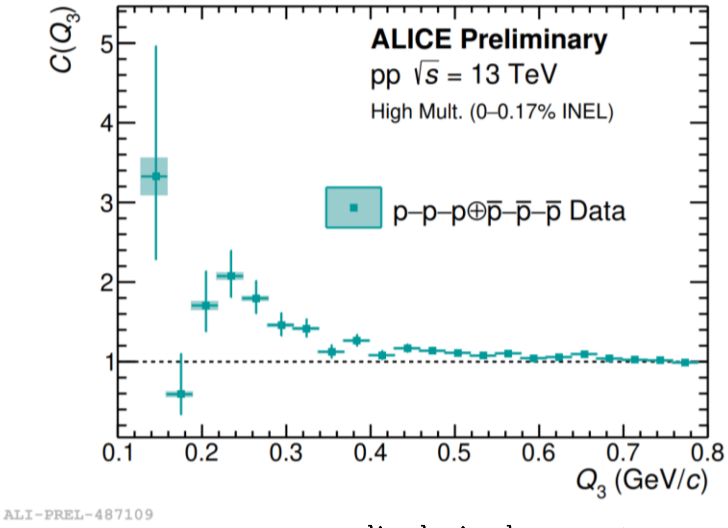


normalised mixed moment
(before subtraction)

# 3-body interactions

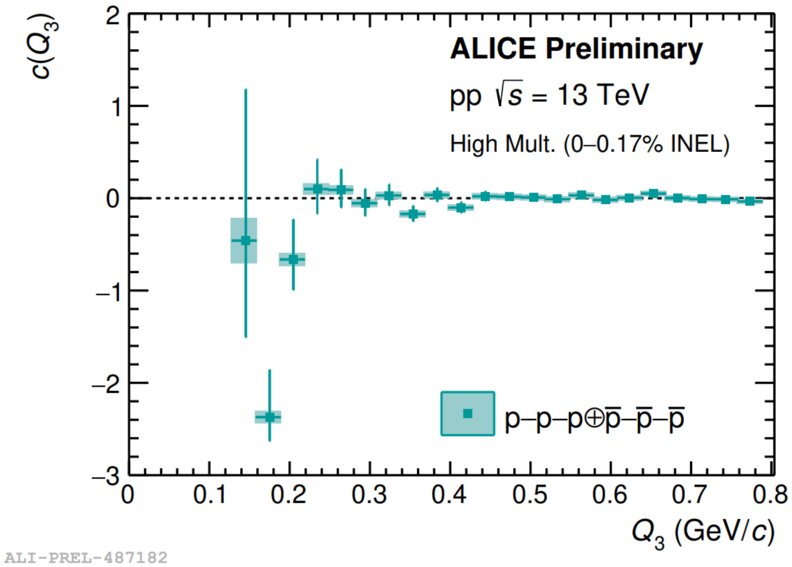


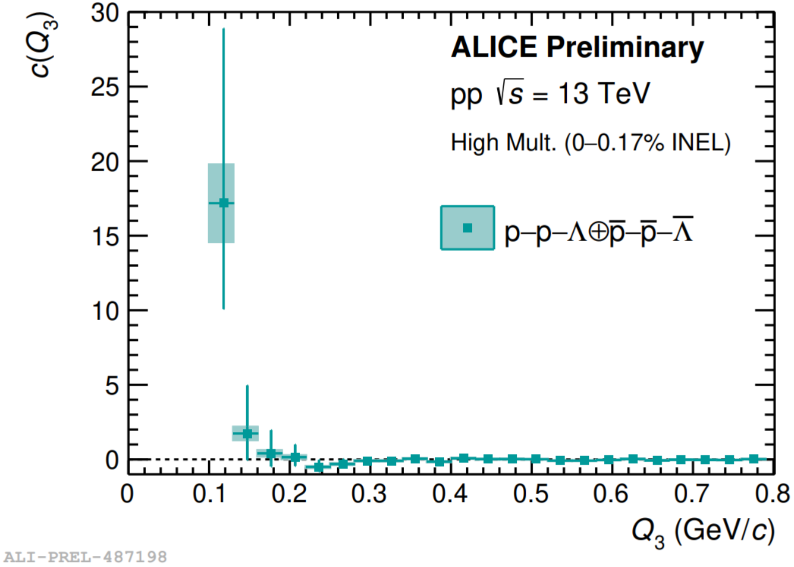


Experimental hint to the presence of an effect beyond the two-body interaction in the p–p–p system

**pp$\Lambda$** no significant deviation observed from the null hypothesis

| RUN I 2009-2013 | LS1 | RUN 2 2015-2018 | **LS2** | RUN 3 2022-2025 | LS3 | RUN 4 2029-2032 | LS4 | RUN 5 2035-2038 | LS5 | RUN 6 2040-2041 |
|---|---|---|---|---|---|---|---|---|---|---|

## LS2 - Phase 1 upgrades

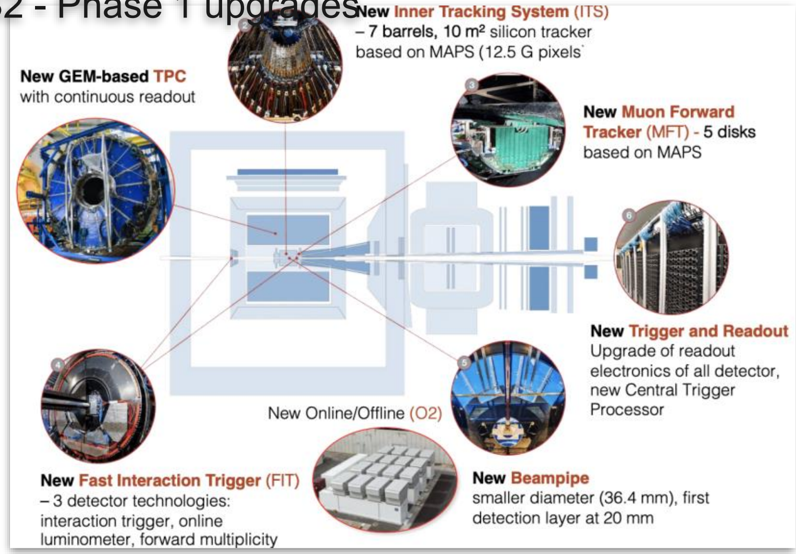


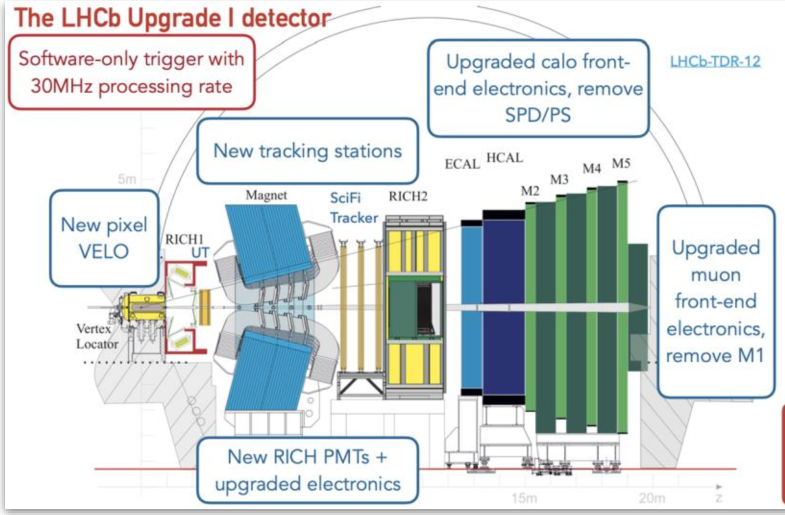


- Less than 10% of the detector channels have been kept
- 100% of the readout electronics has been replaced
- NEW data acquisition system and data center

Very challenging installation and commissioning!

# Upgrade of experiments

RUN I 2009-2013 | LS1 | RUN 2 2015-2018 | LS2 | RUN 3 2022-2025 | **LS3** | RUN 4 2029-2032 | LS4 | RUN 5 2035-2038 | LS5 | RUN 6 2040-2041

ALICE 2.1

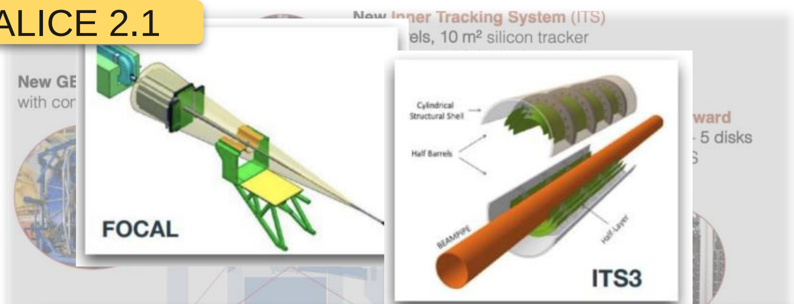


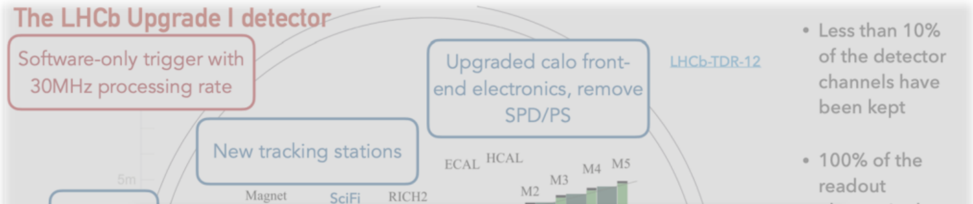


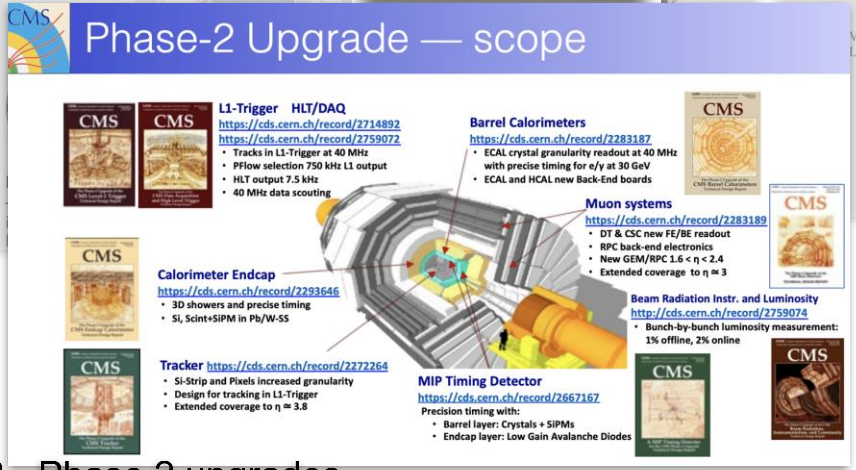


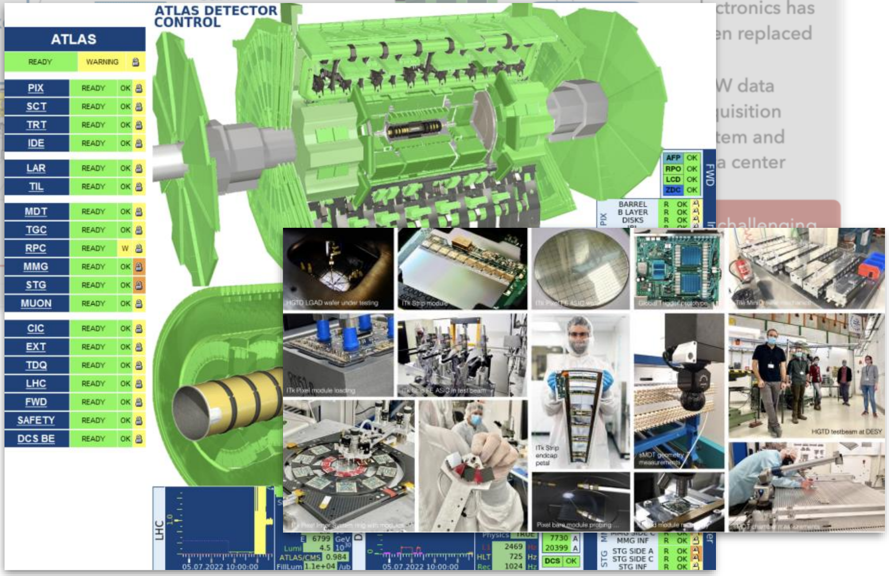


LS3 - Phase 2 upgrades

# Next generation heavy-ion detector: ALICE3

RUN I 2009-2013 | LS1 | RUN 2 2015-2018 | LS2 | RUN 3 2022-2025 | LS3 | RUN 4 2029-2032 | LS4 | RUN 5 2035-2038 | LS5 | RUN 6 2040-2041

**Compact all-silicon tracker**
→ clean separation of signal and background
**Vertex detector** with excellent pointing resolution
→ clean reconstruction of decay chains
**Particle identification**
→ background suppression
**Large acceptance**
→ statistics and correlations
**Superconducting magnet system**
→ effective provision of required magnetic field
**Continuous read-out and online processing**
→ large data sample to access rare signals

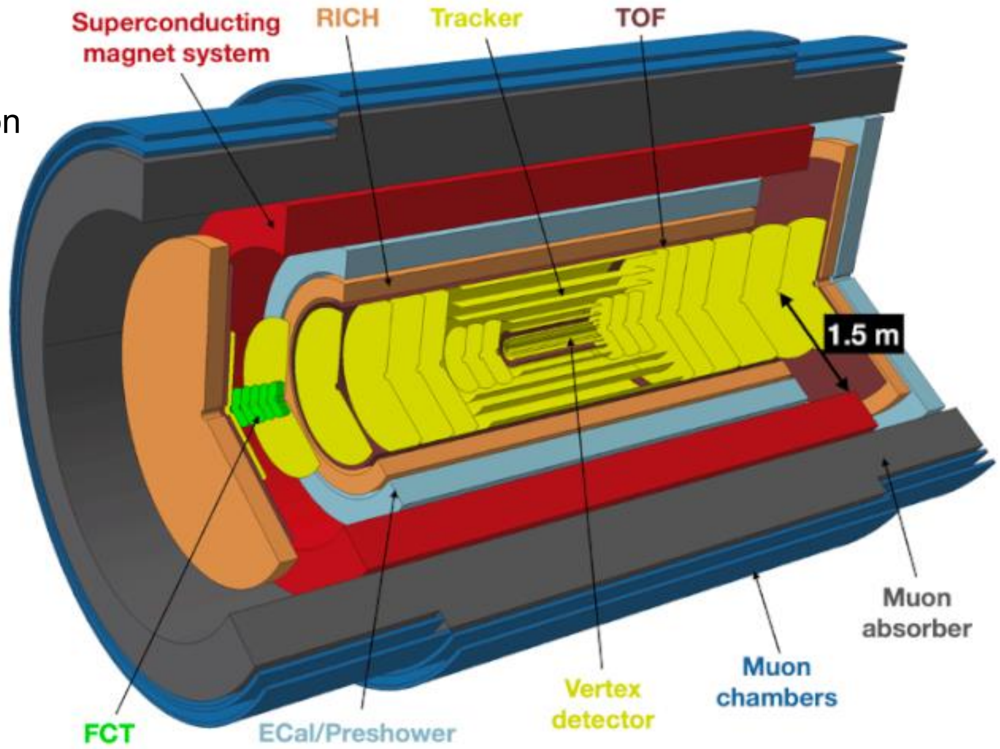

# pp collisions @ 13.6 TeV!